Short-range Forecasting Research

Forecasting Research Division
Technical Report No. 35

STUDY OF CIRRUS CLOUD WINDS: ANALYSIS OF I.C.E DATA

FINAL REPORT FOR EUMETSAT CONTRACT ITT 91/16

by

R.W. Lunnon, D.A. Lowe, J.A. Barnes and I. Dharssi

December 1992

Meteorological Office
London Road
Bracknell
Berkshire
RG12 2SZ
United Kingdom

Forecasting Research Division
Technical Report No. 35

STUDY OF CIRRUS CLOUD WINDS: ANALYSIS OF I.C.E DATA

FINAL REPORT FOR EUMETSAT CONTRACT ITT 91/16

by

R.W. Lunnon, D.A. Lowe, J.A. Barnes and I. Dharssi

December 1992

STUDY OF CIRRUS CLOUD WINDS : ANALYSIS OF I.C.E. DATA FINAL REPORT FOR CONTRACT ITT 91/16

R.W.Lunnon, D.A.Lowe, J.A.Barnes and I.Dharssi

January 8, 1993

EXECUTIVE SUMMARY

Low level satellite cloud motion winds (SCMWs) produced operationally by ESOC are extremely accurate: when verified against numerical analyses the accuracy is very close to that of radiosonde winds. However, high level winds are not so accurate, and it is believed that the major source of error is the height assignment, in particular the semi-transparency correction applied to the radiances from cirrus clouds. During the International Cirrus Experiment (I.C.E.) in 1989, measurements of wind, temperature, humidity and a number of microphysical and radiative parameters were made by up to 5 aircraft flying simultaneously in cirrus cloud. This paper describes the work done using the aircraft data from the experiment together with METEOSAT data to improve our understanding of the dynamical and radiative properties of cirrus clouds, in context of the semi-transparency correction.

The extreme in-cloud vertical wind shear found was about 25 m/s in 100hPa.

In assessing the extent to which cloud motions were representative of the true wind field, it was found that a template size of 16 * 32 pixels (16 pixels in the north-south direction, 32 in the east-west) gave the best results. However it is considered that a template size of 16 * 16 pixels would be the most informative for users. It should be stressed that much of the automatic processing should still take place on segments of 32 * 32 pixels.

The aircraft data were used, amoung other things, to generate so-called Empirical Levels of Best Fit (ELBFs), that is, the level at which the SCMW agrees best with the aircraft wind data.

It was found that the semi-transparency correction was very sensitive both to the incoming radiance data and to the water-vapour channel calibration coefficient. Therefore a vicarious calibration of the water-vapour channel was performed, using the ELBFs. The calibration coefficient arising from this was 10 to 20 %. lower than the operational value. However it should be stressed that different interpretations should be placed on this vicarious value and the operational value, and consistency should not be expected a priori. Furthermore it was shown that, because of the sensitivity the semi-transparency correction to the incoming data, and because the correction is not performed if the water vapour channel radiance, converted to physical units, is too high, the best results are to be obtained using the operational value.

Recommendations are made for calibration/validation procedures, using either radiosonde data or the combination of in situ measurements and dropsonde data from the Uk Met Office C-130. Suggestions are made for the future approaches to the height attribution of semi-transparent clouds.

1 Introduction: Satellite Cloud Motion Winds (SCMWs)

SCMWs, are produced operationally by all the operators of geostationary meteorological satellites. The low level SCMWs produced operationally by ESA from METEOSAT data (Schmetz et al, 1992) are extremely accurate: when verified against numerical analyses the accuracy is very close to that of radiosonde winds (Thoss, 1992). However, high level winds are not so accurate, when compared with radiosonde winds. Sources of error in SCMWs can be split into the following areas

- Image navigation - the fact that there is an error in the earth-referenced position of a point in the image.
- Image contamination - ideally images should comprise a selection of well defined tracers against a completely uniform background, but in practice, particularly for high level clouds, this is rarely the case.
- Tracking error - a tracer will be tracked without error only if pixels in all the requisite images comprise either entirely tracer or entirely background, and the tracer moves without changing its shape in any way.
- The combined effects of height attribution error and the tendency for cloud motion not to be representative of wind at cloud top.
- The use of an inappropriate form of ground truth. Operational SCMWs from ESA in mid-latitudes are representative of spatial sales of approximately 160 * 300 km and time scales of one hour. They are often compared with other sources of wind information which are representative of smaller space and time scales.

Lunnon and Lowe (1990) showed that there was significant correlation between the error in SCMWs and the vertical wind shear. This, together with the acknowledged accuracy of low-level SCMWs, leads us to believe that the major source of error is the height assignment, in particular the semi-transparency correction applied to the radiances from cirrus clouds. A further complication is that cirrus clouds may not move with the wind at the cloud top. Thus complete understanding of the problem involves dynamics, microphysics and radiative transfer theory. During the International Cirrus Experiment (I.C.E.) in 1989, measurements of wind, temperature, humidity and a number of microphysical and radiative parameters were made by up to 5 aircraft flying simultaneously in cirrus cloud. As will be explained in the next section, three of those aircraft were considered the most critical for processing. Thus the data obtained provided the best opportunity to study the problem of the semi-transparency correction using contemporaneous observations of all the relevant variables.

Section 2 of this paper gives more details of the I.C.E. experiment, with details pertaining to the particular missions chosen for study in this project. Section 3 makes use of the aircraft data to consider the vertical and horizontal wind shear in and near cirrus clouds. Section 4 compares cirrus motion vectors (obtained from the satellite data) with the true wind (from the aircraft data) on a variety of scales. Section 5 describes the application of the operational (as used by ESOC) semi-transparency correction to data from the I.C.E. experiment. Section 6 makes recommendations for the calibration and validation of both winds and radiances. Section 7 comments on future approaches to the height attribution of semi-transparent clouds. An appendix discusses the generation and selection of model atmospheres, which is part of the process of generating the semi-transparency correction.

2 The use of data from the International Cirrus Experiment (I.C.E.)

2.1 Rationale

The I.C.E. experiment was originally perceived as part of the International Satellite Cloud Climatology Project, but is now organised within the European Cloud Radiation Experiment (EUCREX). The major field campaign was carried out between 18th September and 20th October 1989 in the southern part of the North Sea. Intensive observations were made by ground-based and airborne systems, and extensive use has subsequently been made of satellite data. Thus the specialised observations collected during the I.C.E. experiment offer a unique opportunity to improve our understanding of the dynamics and radiative properties of cirrus, hopefully enabling more accurate SCMWs to be generated operationally in the future. The study made use only of the aircraft data (in conjunction with satellite data and archived operational numerical forecast data). Originally it had been intended that radiation data from the C130 would be used, specifically because they have enhanced spatial resolution compared with the satellite data. However at an early stage it was decided to use METEOSAT visible data to provide this extra resolution instead: this has the clear advantage that if the use of such data proves valuable, it could be incorporated into operational practices (at least, during daytime).

Although a maximum of five aircraft were flying at any one time in the experiment, data from only three of them were used. Of the other aircraft, the Dornier 228 operated by DLR was considered to be flying too low to contribute useful information (on only two missions did it fly above flight level 120, approximately 12000 feet) and the Egrett operated by the Weltraum-Institute in Berlin flew too high, too infrequently and was not appropriately instrumented to provide useful data. The factors considered when selecting missions were the availability of satellite and aircraft data, whether all three aircraft (the Falcon operated by DLR, the Merlin operated by Centre d'Aviation Meteorologique, and the C130 Hercules operated by Meteorological Research Flight) were flying colocated patterns, the synoptic situation and the likelyhood of being able to generate SCMWs, which was determined by examining the histograms of infra-red radiances. In a typical mission, the Merlin would be flying at about flight level 220, the C130 at about flight level 260 and the Falcon at about flight level 300. The following were the chosen missions, together with the MIEC calibration coefficients taken from METEOSAT calibration reports (ESOC, 1989 & 1990). The Julian day is shown in this table for convenience in cross-refering to the calibration reports.

Mission	*Date*	*Julian Day*	*Infra − red Calibration Coefficient*	*WaterVapour Calibration Coefficient*
ICE − 201	18*th September* 1989	261	0.06760	0.0082
ICE − 202	20*th September* 1989	263	0.06723	0.0081
ICE − 207	28*th September* 1989	271	0.06794	0.0082
ICE − 208	10*th October* 1989	283	0.07022	0.0085

Originally it had been intended to consider missions 209, 210, 211 and 215. However for mission 209 the WV imagery were corrupted, so this was disregarded. Mission 210 was rejected because the Falcon and C130 were not flying colocated patterns. Mission 211 was the aircraft intercomparison exercise, conducted in relatively cloud free conditions, and therefore unsuitable for the generation of SCMWs. However, data from it were used to refine the algorithm for processing wind data from the C130 so that they were consistent with data from the Falcon. Mission 215 was disregarded because the aircraft were not flying colocated patterns. Note that the data for the Merlin for mission 208 arrived too late for inclusion in the processing.

Of course METEOSAT imagery (all three channels, at half hourly intervals covering the periods when all three aircraft were flying) were also used.

2.2 Synoptic situation for ICE201

The synoptic situation for mission 201 was as follows. A ridge of high pressure over Germany and a trough lying over the Atlantic leads to a weak southwesterly airflow advecting warm air into the area over the North Sea. A strong depression lies north-west of Ireland and a weak warm front stretches from the north of Scotland to Denmark. The experimental area was selected in this warm frontal region to the west of Denmark where the front had associated cirrus cloud with altostratus underneath.

2.3 Synoptic situation for ICE202

Ahead of a strong stationary trough but also under the influence of a weak ridge axis lying roughly over France and Germany, a west-south-westerly airflow is advecting warm air at upper levels to the experimental area. A depression just south of the Faeroe Islands is moving quickly north-eastwards with its associated warm front

just touching the north of the experimental area. As a result thick cirrus ahead of this frontal system occurs in the northern part of the North Sea with patchy multi-levelled cirrus further south moving eastwards and dissipating over the Danish coast. In this mission the aircraft moved east from original coordinates to try and follow cloud motion.

2.4 Synoptic situation for ICE207

Expermental area was situated between strong high over the Atlantic and deep trough and affected by a north by westerly airflow. The area has just been passed by a cold front and is ahead of a surface warm front approaching from the north west. At the start of this mission strong warm advection in the northern part of the North Sea. Later on in the day dense cirrus approached from the west.

2.5 Synoptic situation for ICE208

Operational area has just been passed by a sharp trough and is affected by a north by westerly airflow as a jet from the Faeroe Islands to the tip of Norway branches off over the North Sea towards Belgium. Cirrus can be found in connection with this jet and a warm front moving south-eastwards into the North Sea. Aircraft found several patches of multi-layered cirrus with stratocumulus/altocumulus below. The cirrus was dying out towards the end of the experiment.

2.6 Figures relating to particular missions

A number of figures are shown to illustrate various aspects of the different missions. These figures all have a three level figure number such that the last level is indicative of the mission number. The surface synoptic charts are shown in figures 2.1. That is to say, figure 2.1.1 shows the surface synoptic chart for mission ICE201, figure 2.1.2 relates to mission ICE202, figure 2.1.3 relates to ICE207 and figure 2.1.4 relates to ICE208. Figures 2.2 show the 300mb chart for each mission. Figures 2.3 show the segment used to generate most of the winds (for most missions slightly different segment positions were used at different times), and an idealisation of the aircraft flight pattern. Figures 2.4 show the detailed flight track of the C-130: this is shown to illustrate the departure from the idealisation shown in figures 2.3. Figures 2.5 show a typical IR histogram for the processed segment for a representative time.

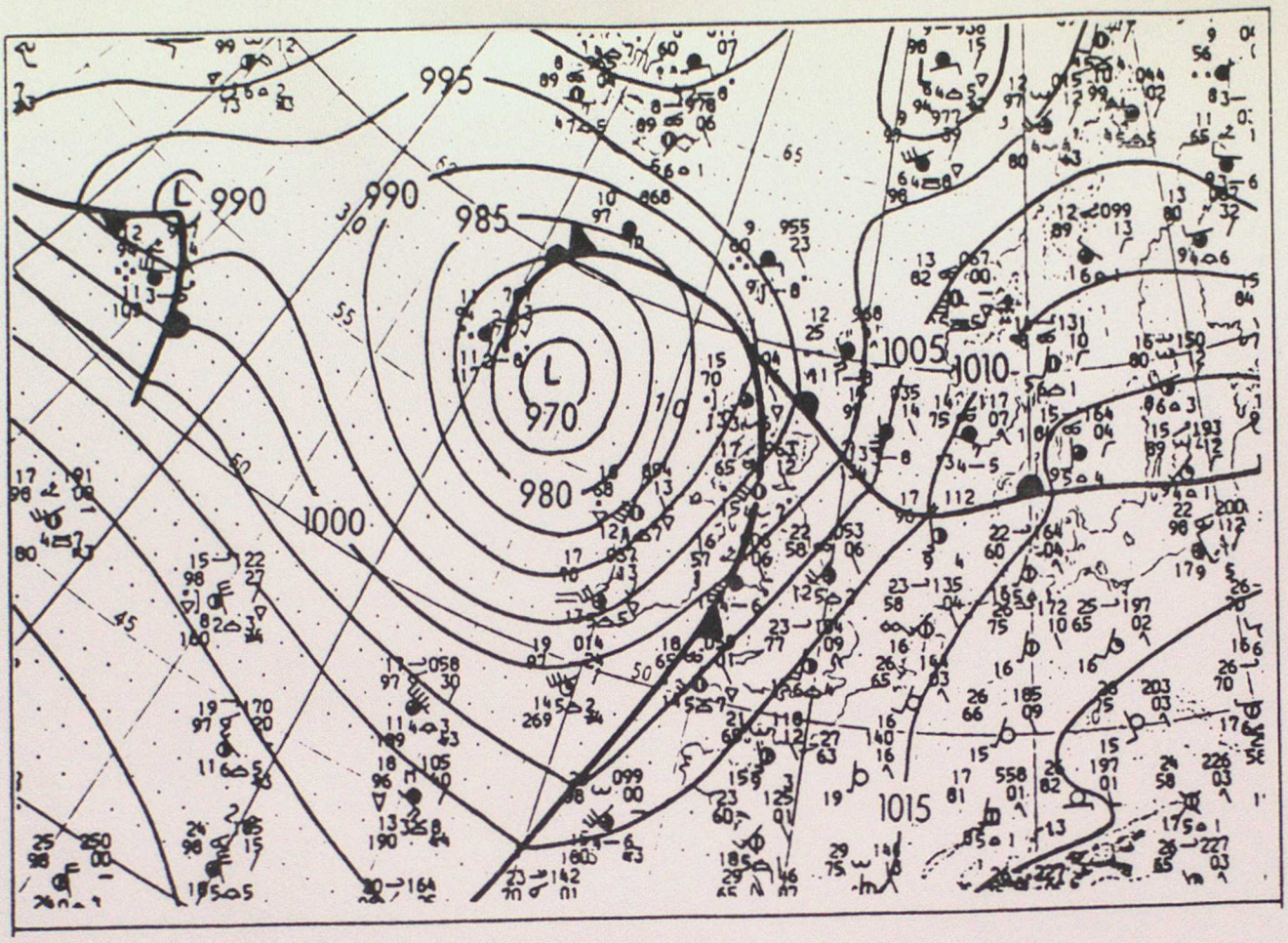

FIGURE 2.1.1 SURFACE 18.09.1989 12Z

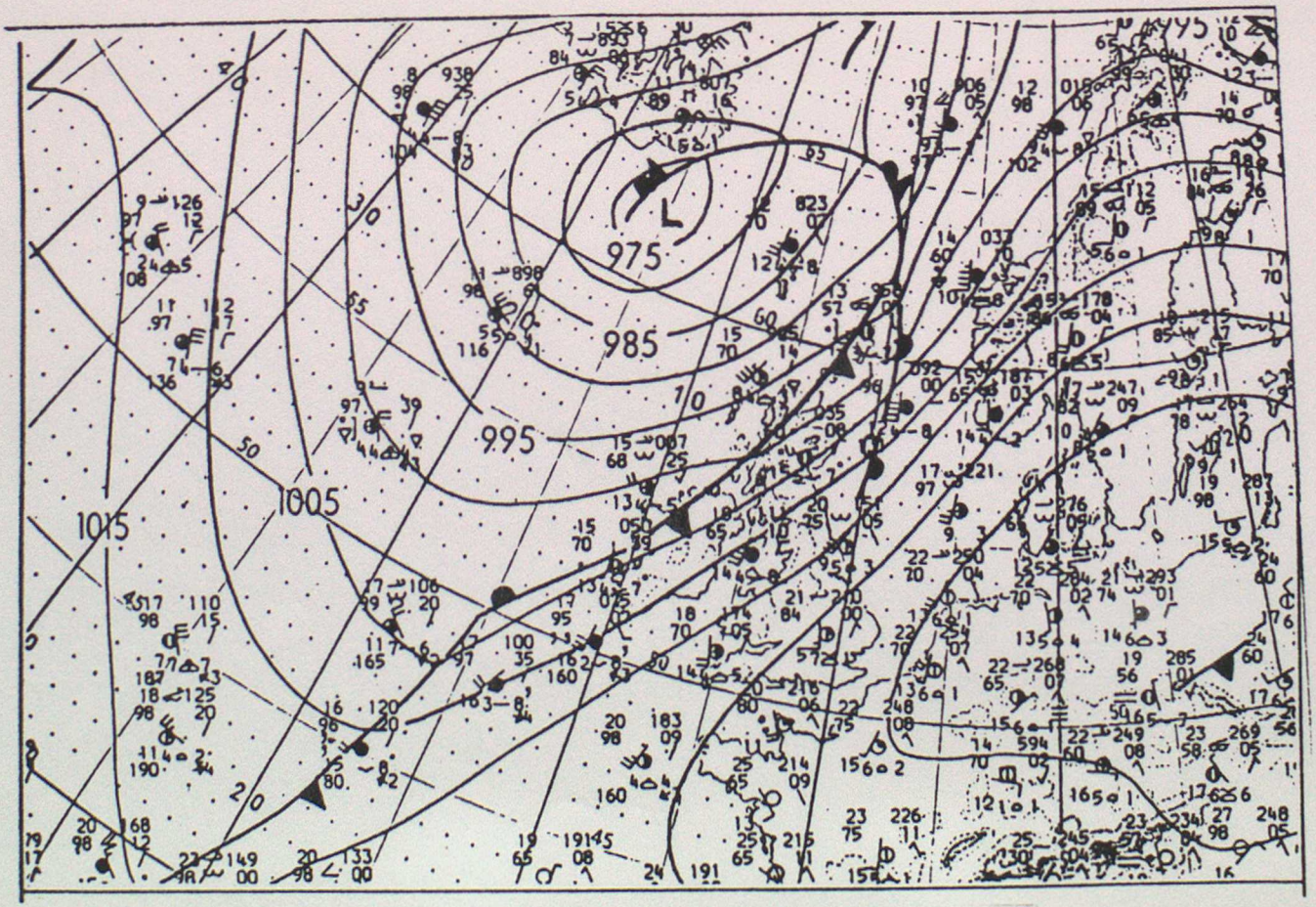

FIGURE 2.1.2 SURFACE 20.09.1989 12Z

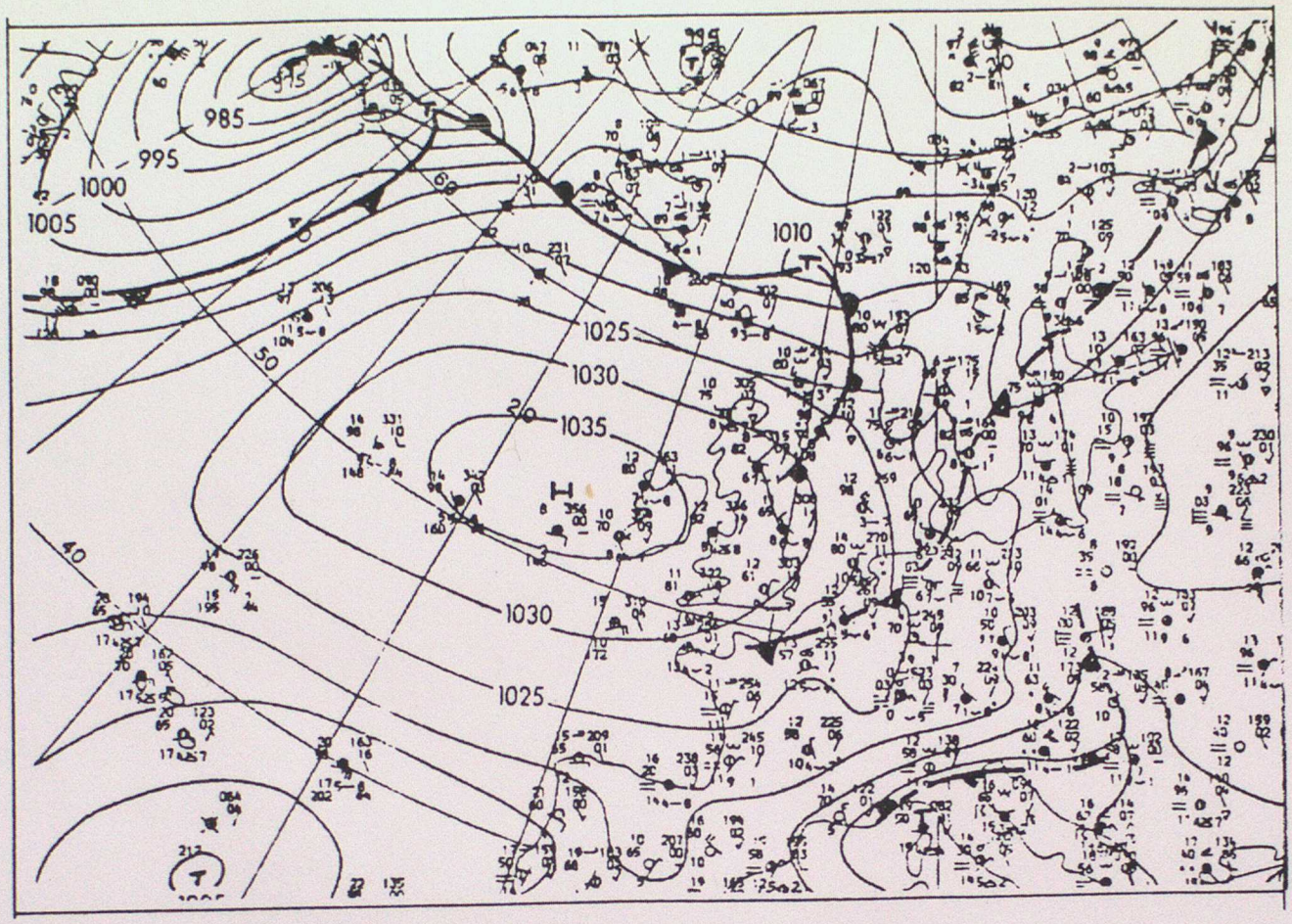

FIGURE 2.1.3 SURFACE 28.09.1989 06Z

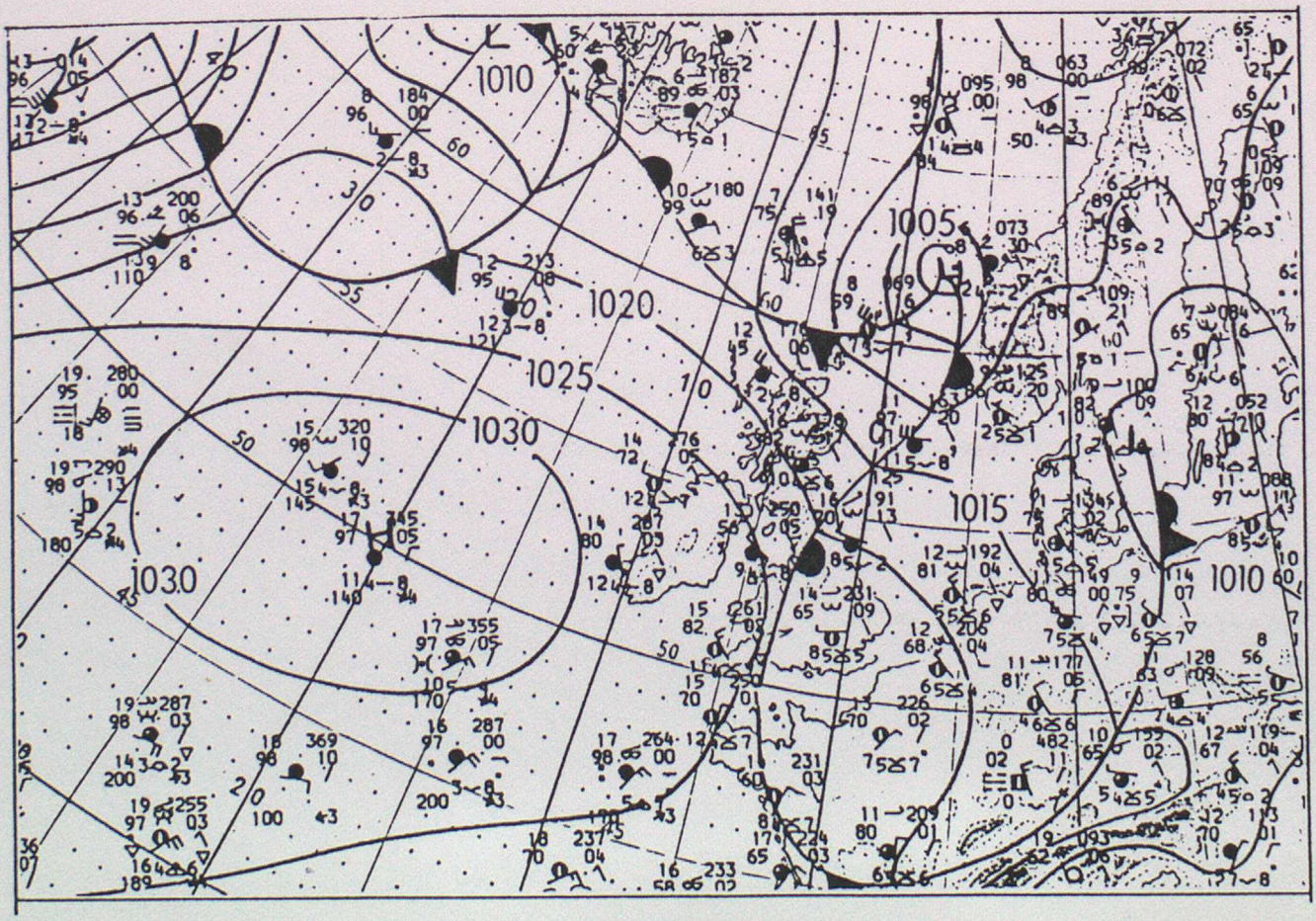

FIGURE 2.1.4 SURFACE 10.10.1989 12Z

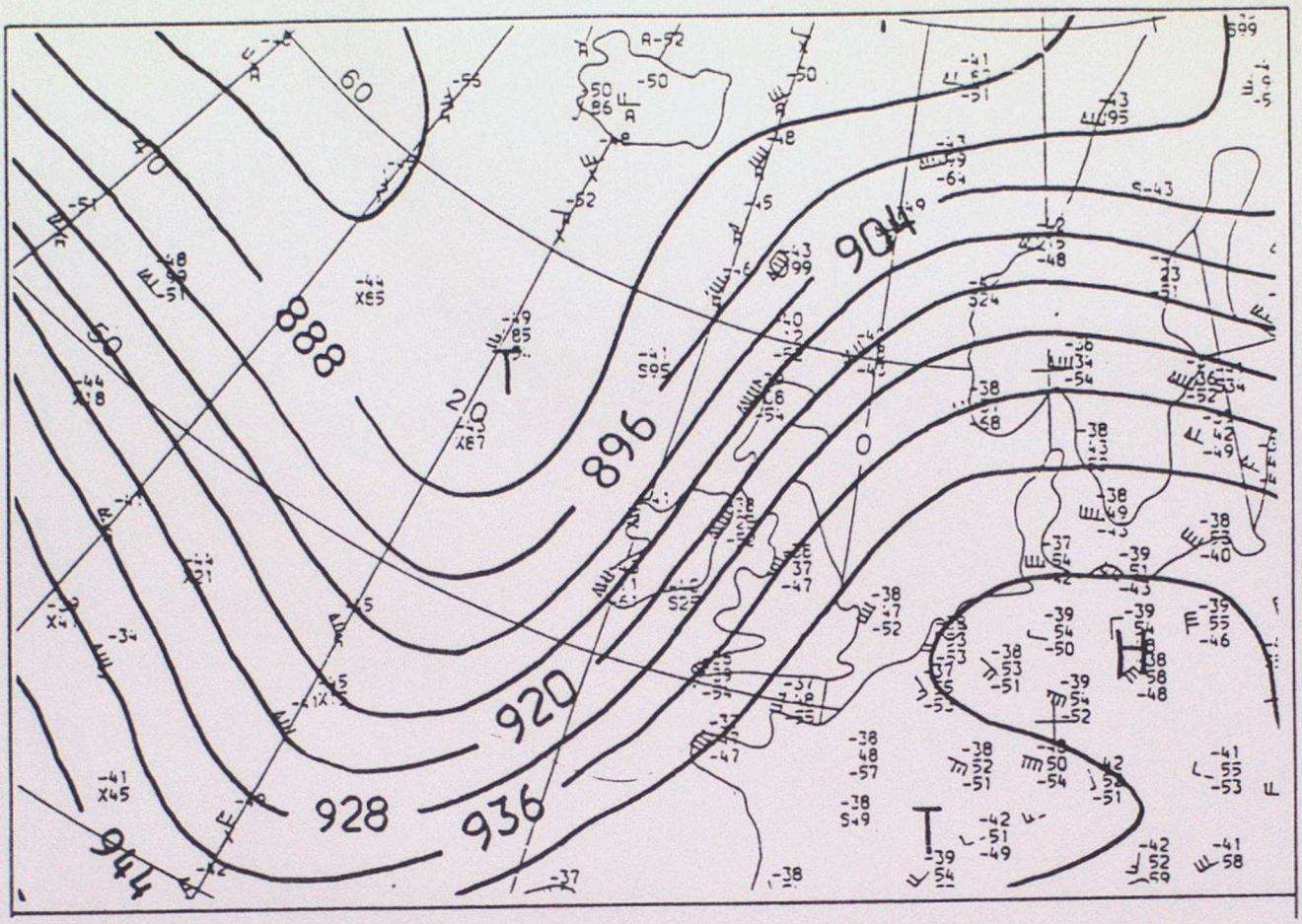

FIGURE 2.2.1 300 MB 18.09.1989 12Z

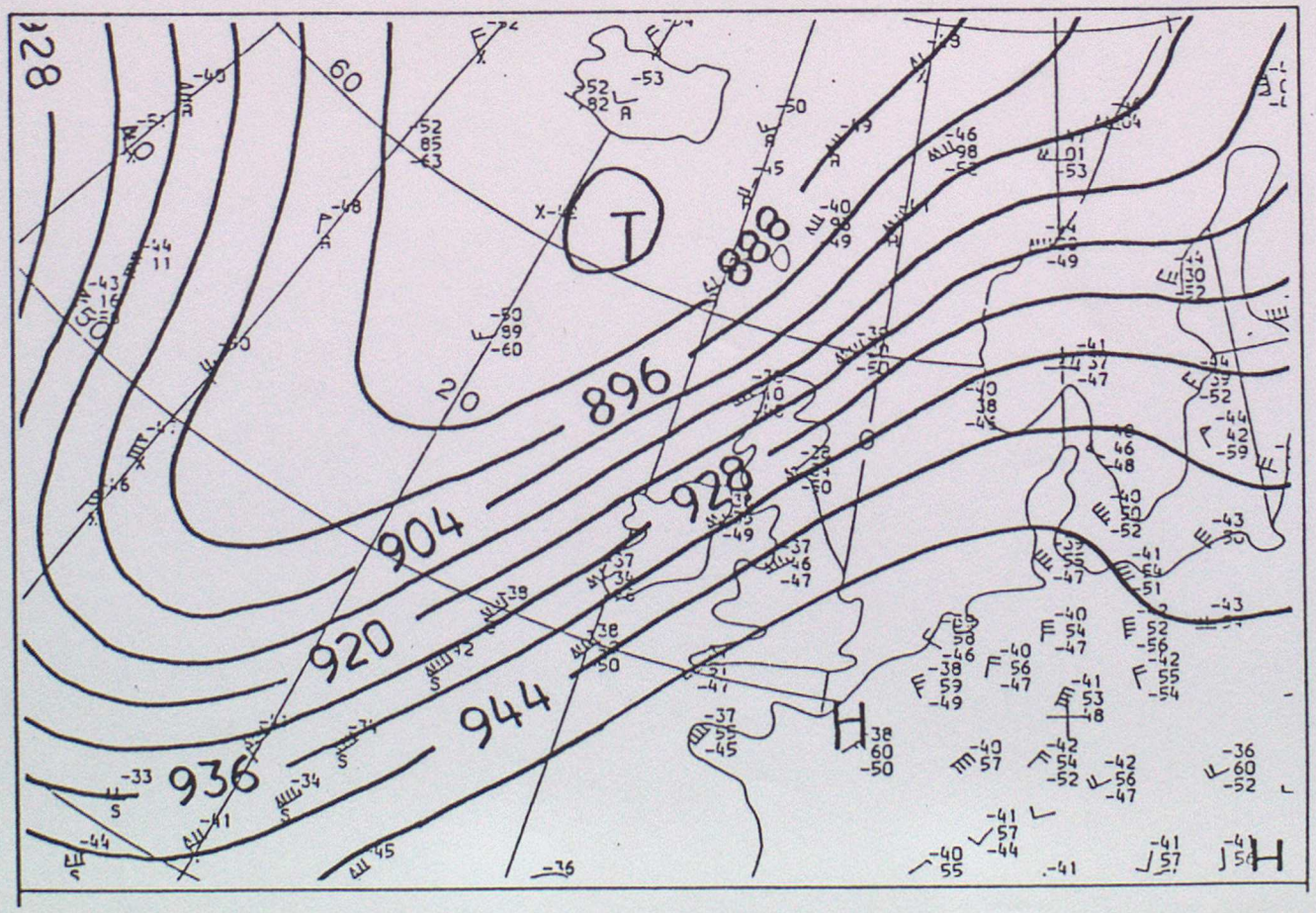

FIGURE 2.2.2 300 MB 20.09.1989 12Z

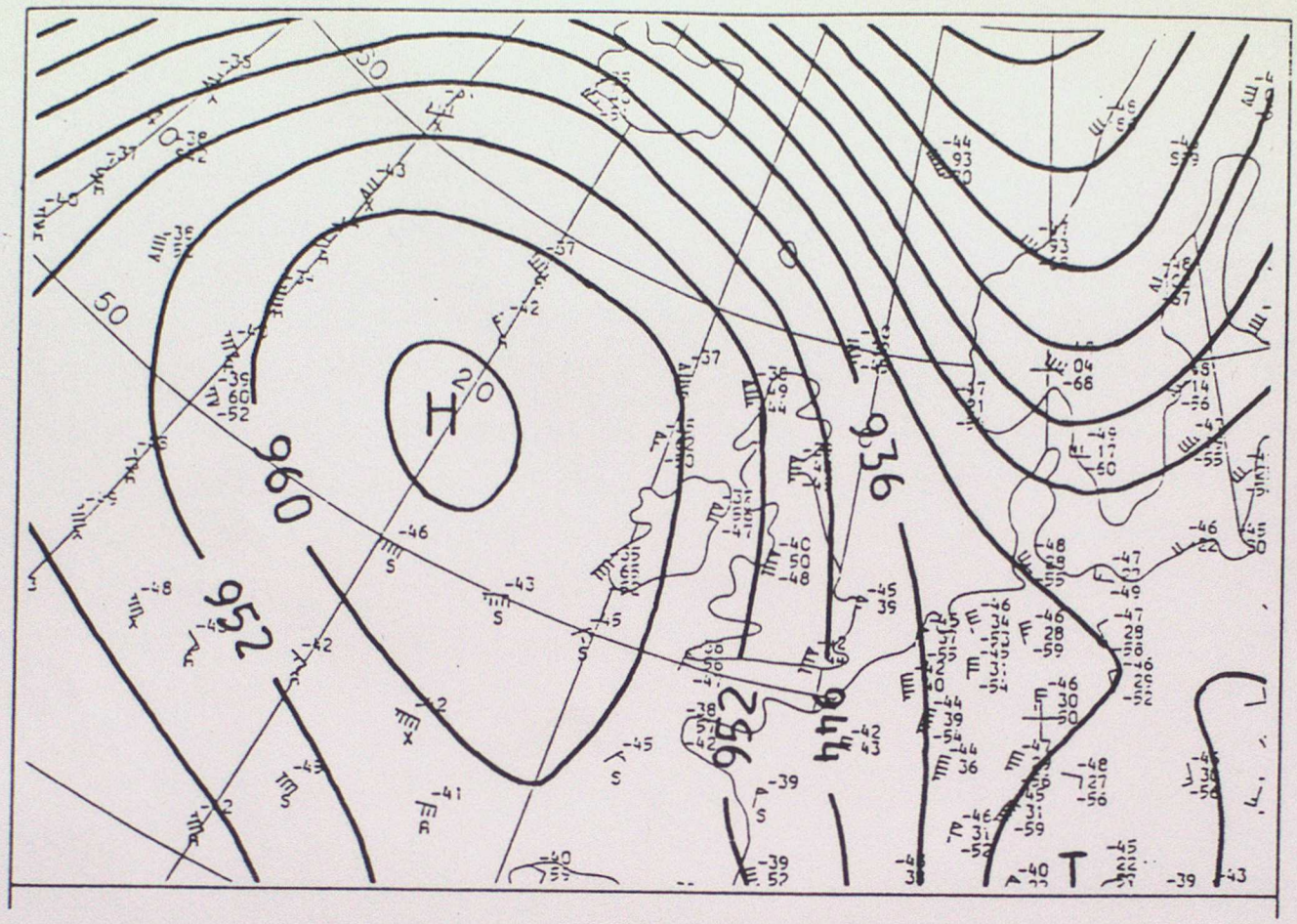

FIGURE 2.2.3 300 MB 28.09.1989 12Z

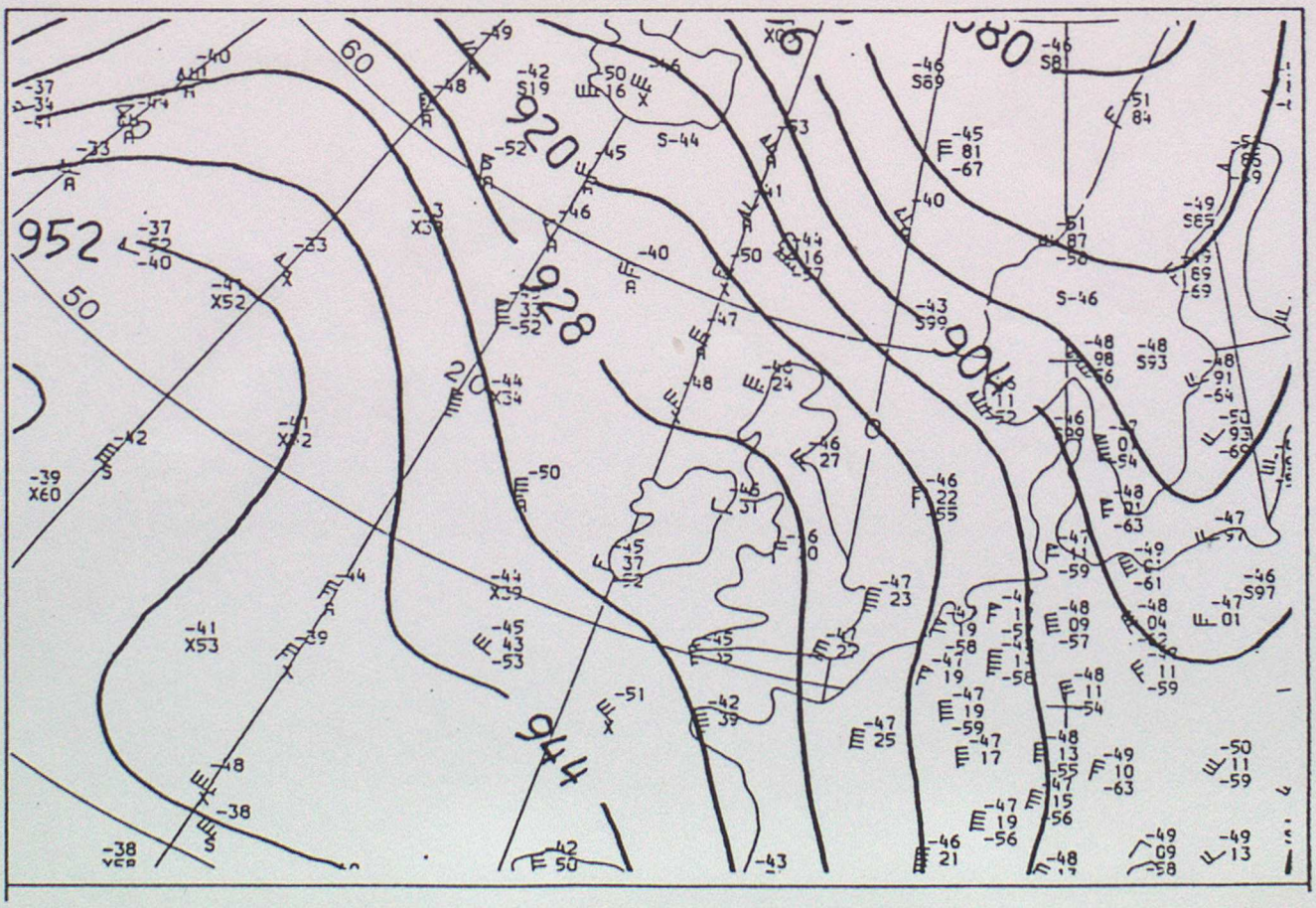

FIGURE 2.2.4 300 MB 10.10.1989 12Z

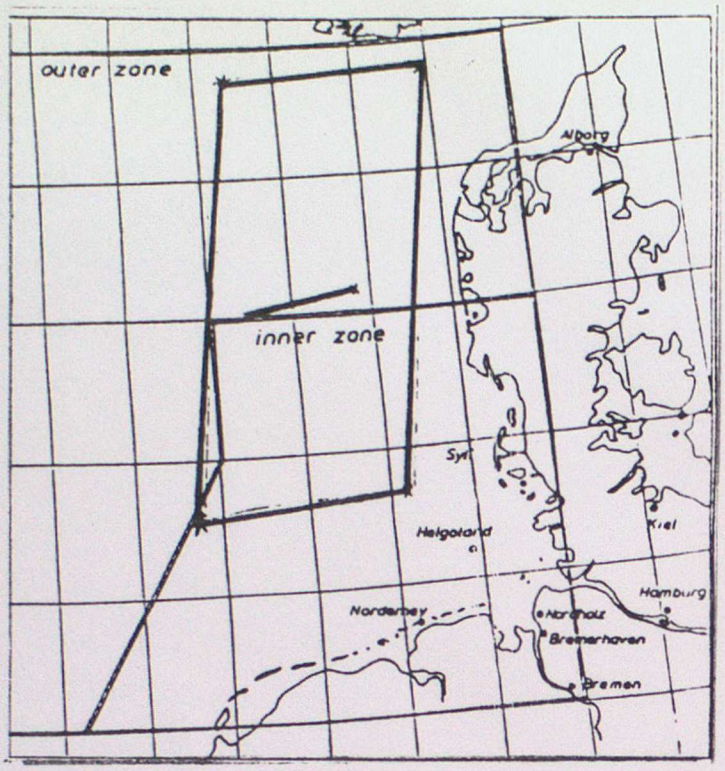

FIGURE 2.3.1 ICE-201

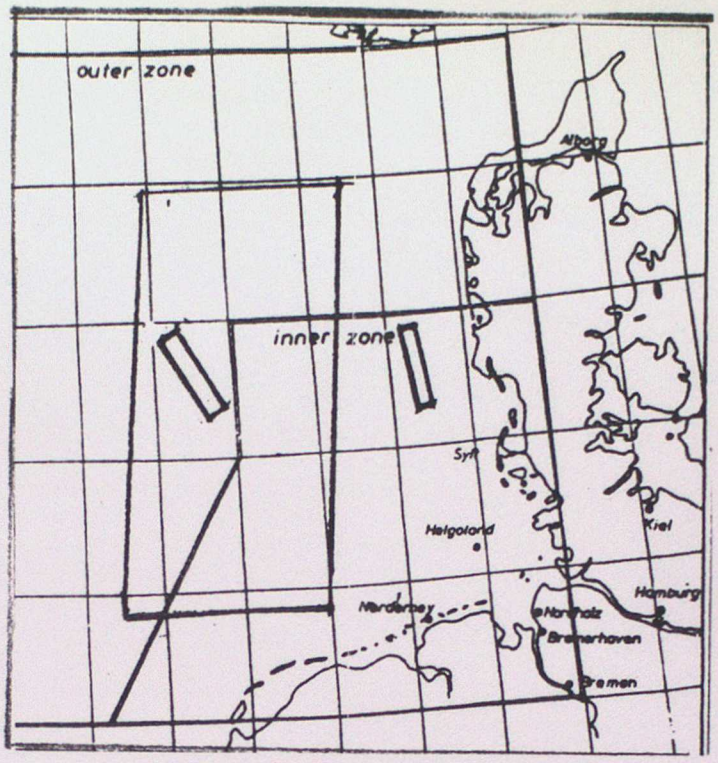

FIGURE 2.3.2 ICE-202

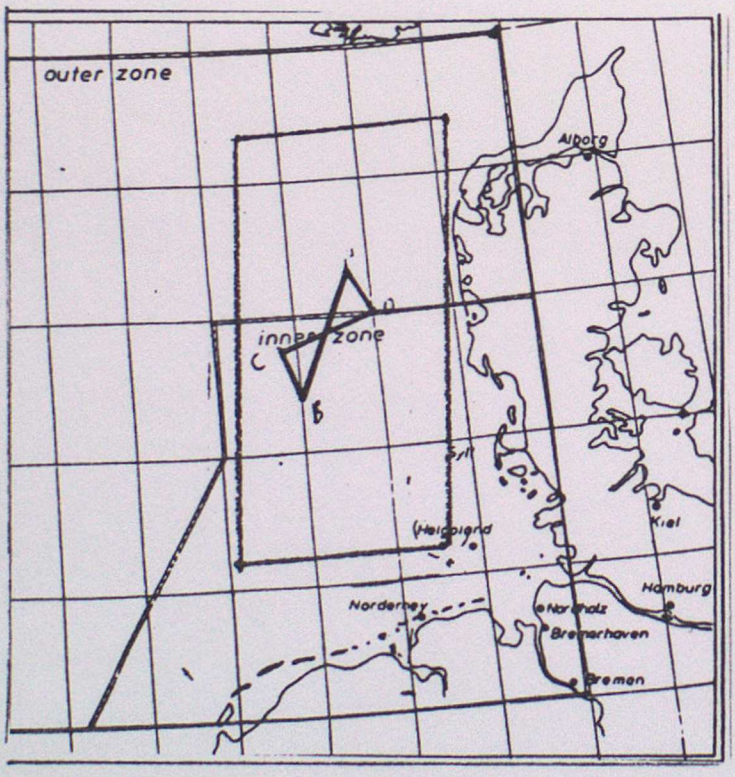

FIGURE 2.3.3 ICE-207

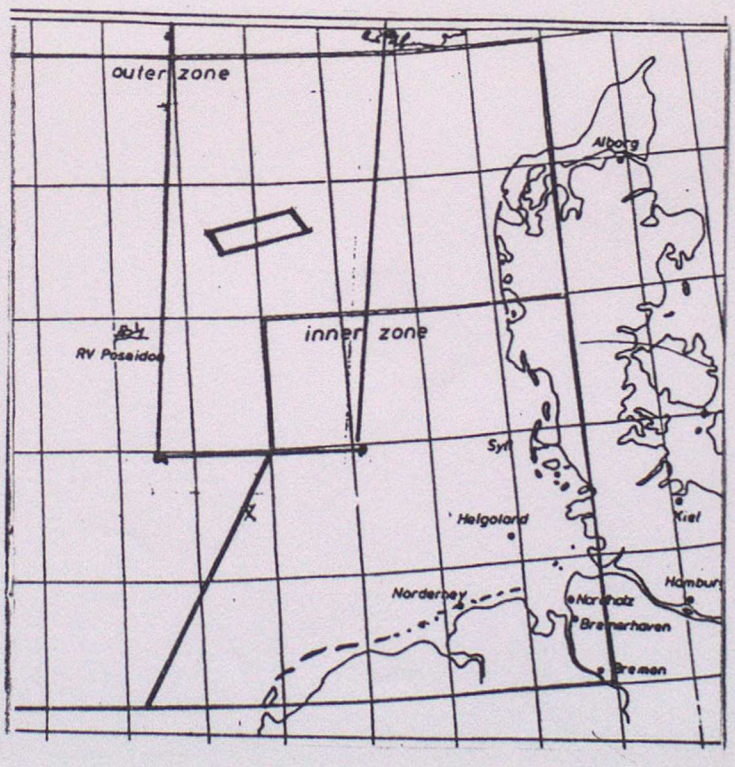

FIGURE 2.3.4 ICE-208

AIRCRAFT TRACK AND TARGET METEOSAT SEGMENT (32*32 IR PIXELS)

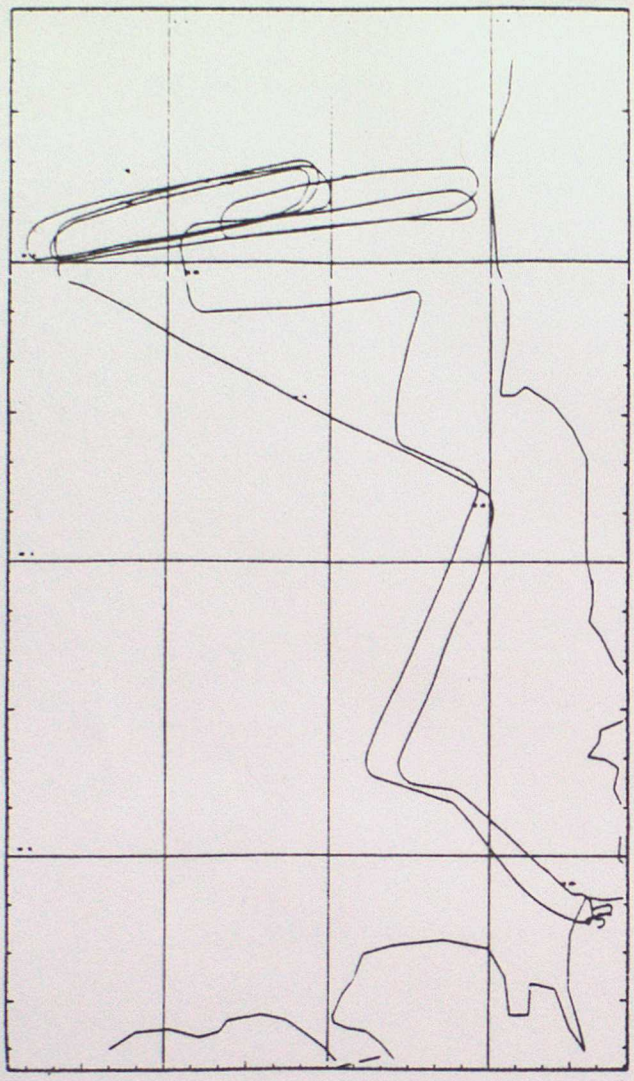

FIG. 2.4.1 C-130 TRACK FOR ICE-201

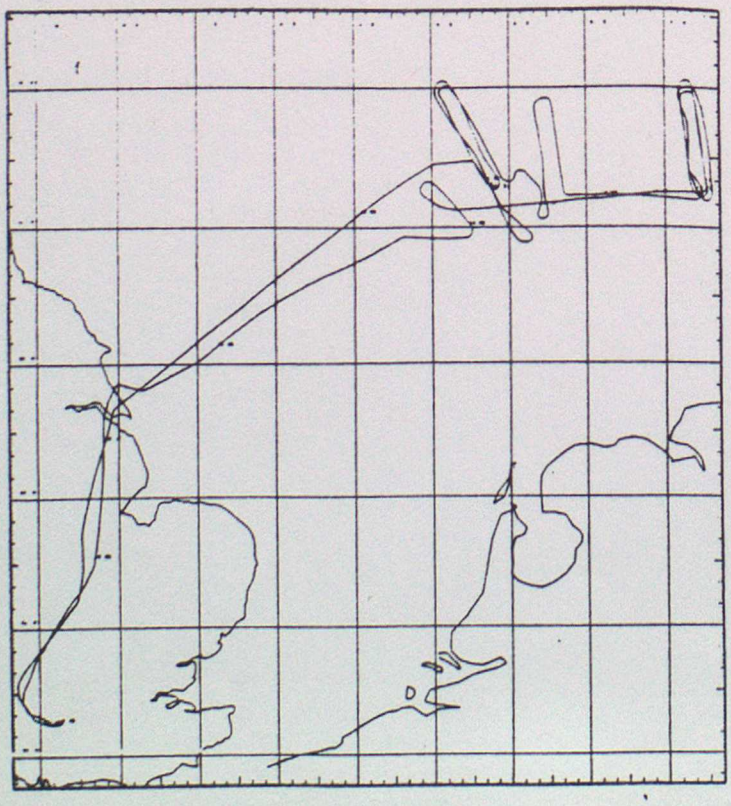

FIG. 2.4.2 C-130 TRACK FOR ICE-202

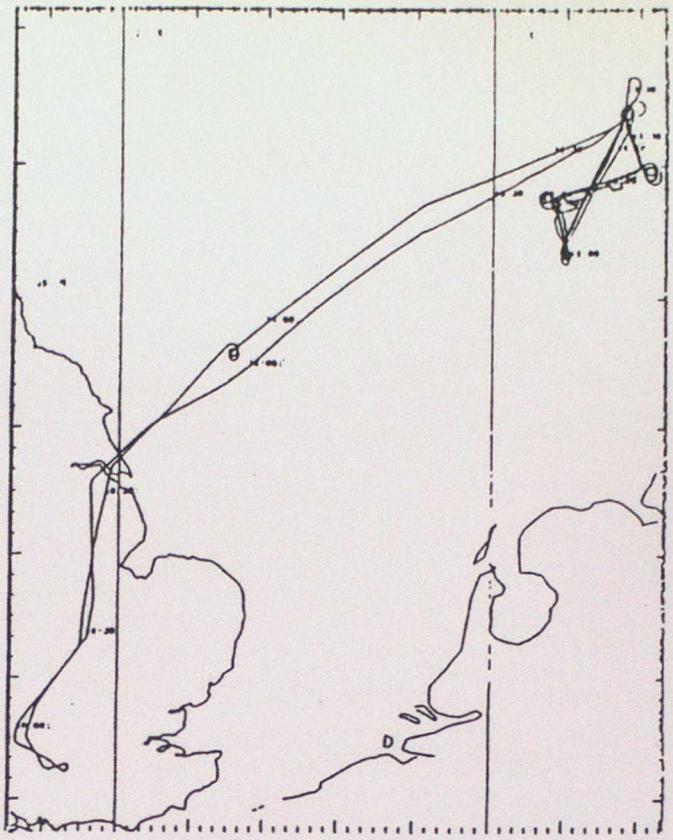

FIG. 2.4.3 C-130 TRACK FOR ICE-207

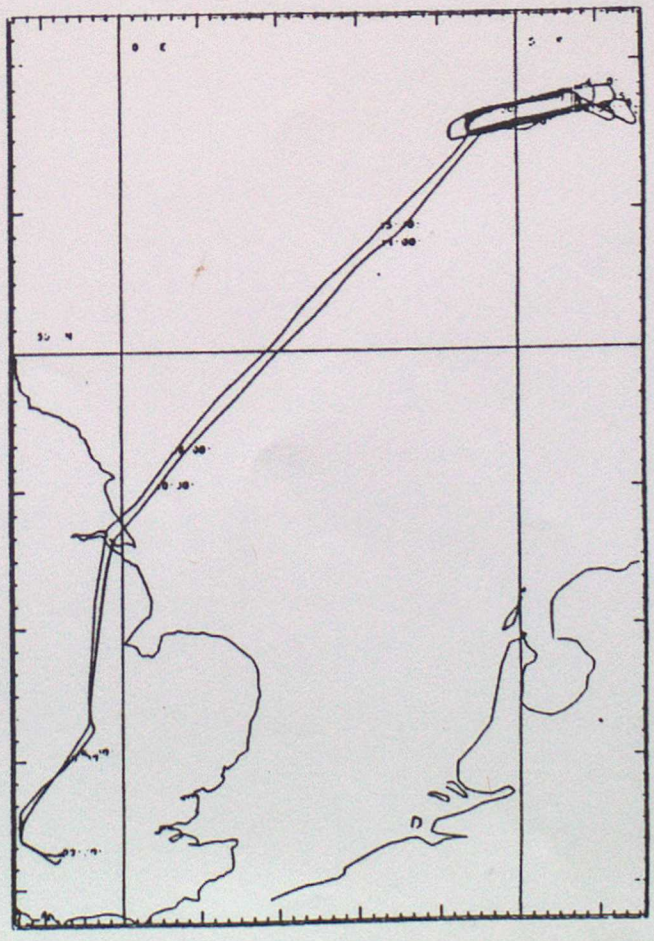

FIG. 2.4.4 C-130 TRACK FOR ICE-208

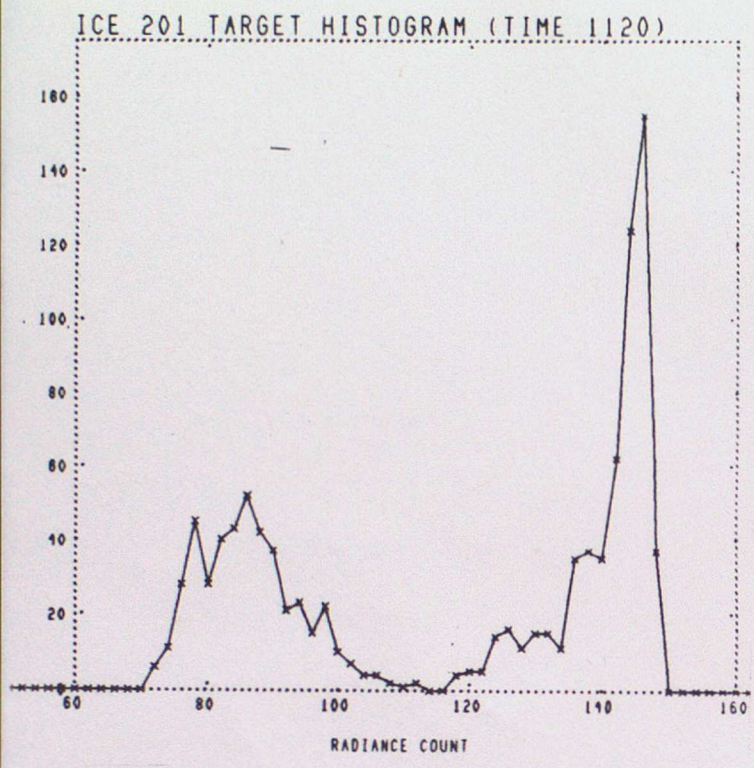

FIGURE 2.5.1

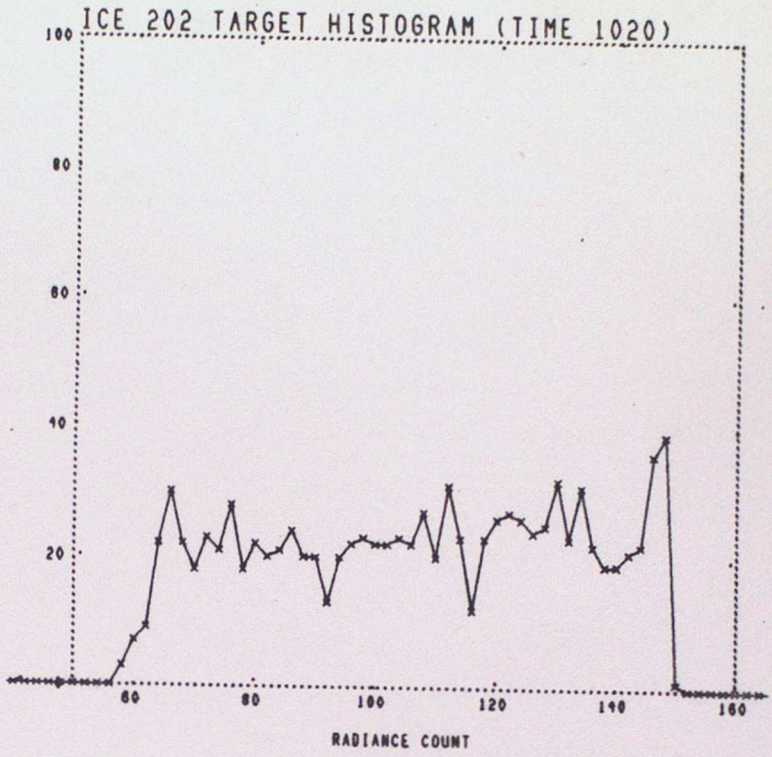

FIGURE 2.5.2

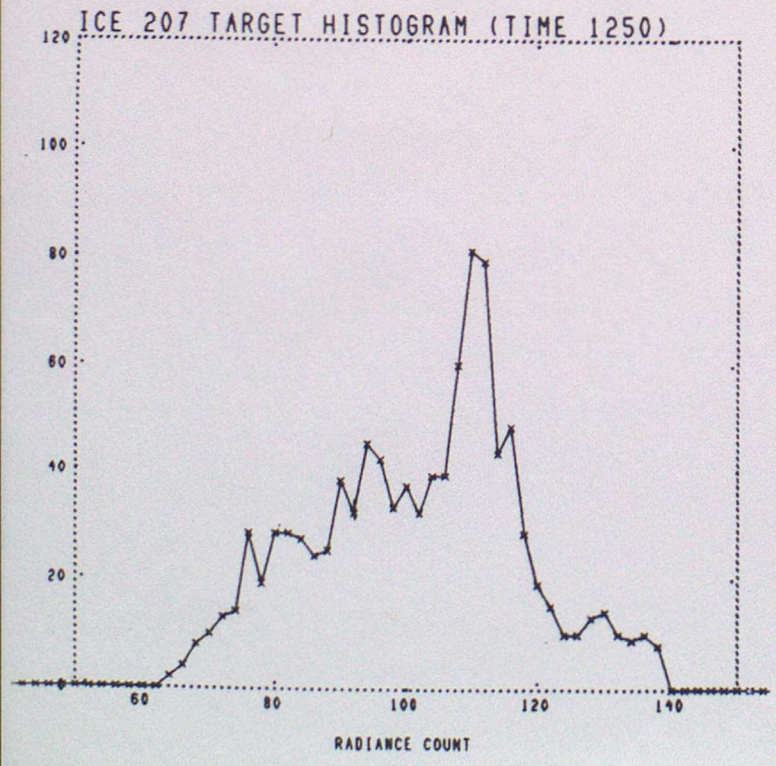

FIGURE 2.5.3

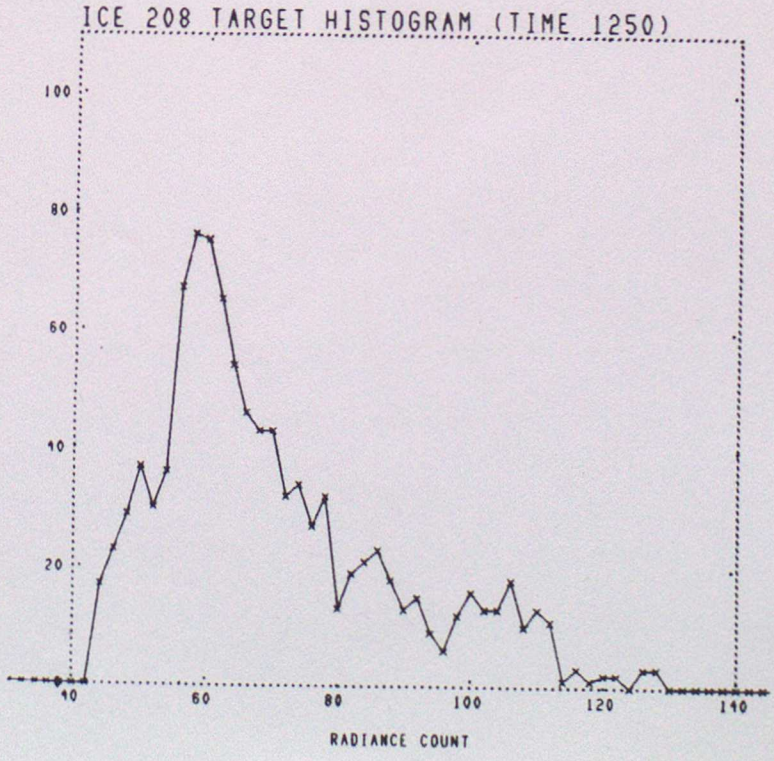

FIGURE 2.5.4

3 Vertical and horizontal wind shear in and near cirrus clouds

3.1 Theoretical considerations

It is worth considering, from a theoretical viewpoint, the relationship between both vertical and horizontal windshear and vertical motion. For mid-latitude synoptic scale vertical motion, Q-vector theory is a useful framework to apply (see Hoskins and Pedder (1980)). The definition of Q_x is as follows:

$$Q_x = -\frac{\partial u}{\partial x}\frac{\partial \theta}{\partial x} - \frac{\partial v}{\partial x}\frac{\partial \theta}{\partial y} \tag{1}$$

Making use of the thermal wind relationship (and the basis of Q-vector theory is that the atmosphere acts to preserve thermal wind balance) we can obtain

$$Q_x \propto -\frac{\partial u}{\partial x}\frac{\partial v}{\partial z} + \frac{\partial v}{\partial x}\frac{\partial u}{\partial z} \tag{2}$$

Where the vector Q field is convergent, one would expect ascending vertical motion, although the relationship is not quite as simple as this because the divergence of Q is equal to a weighted laplacian of the vertical motion field. Nevertheless, it can be said that the forcing of vertical motion is proportional to the product of the vertical and horizontal wind shear. It follows from this that for newly formed cirrus there will be both vertical and horizontal windshear at some location not far from the cloud itself. This will not apply to cirrus formed from the outflow from large convective systems. Also cirrus can be quite long-lived, and the windshear responsible for its formation may dissipate long before the cloud itself.

3.2 The basic processing of the aircraft wind, temperature and humidity data

The analysis was performed on a grid of $40km$ in the horizontal and standard pressure levels in the vertical, and separate analyses were performed at half-hourly intervals, at the times for which the correlation surfaces were produced (see section 4). Note though that aircraft observations influence the analysis at times other than that of the observation itself, so there will be significant correlation between the analyses at the different times. This will also occur because the analysis uses as background information the operational fine-mesh analyses (Bell and Dickinson, 1987), which are made every three hours and are interpolated to provide data at half-hourly intervals. The system used to analyse the aircraft wind, temperature and humidity data is the WAFTAGE (Winds Analysed and Forecast for Tactical Aircraft Guidance over Europe) system, essentially as described in Lunnon (1991). The basic method used is optimum interpolation, which forms the basis for nearly all operational data assimilation schemes.

3.3 Cross-sections of wind, humidity and satellite radiance from I.C.E. experiment

Figures 3.1.1, 3.1.2, 3.1.3 and 3.1.4 are high-resolution cross sections of wind speed for missions 201,202,207 and 208 respectively. The orientation of the cross section was chosen to be roughly perpendicular to the upper flow, as it was considered that such an orientation would have the best chance of portraying the horizontal wind shear. Cloud boundaries are also shown, but these should be regarded as being somewhat subjective, for the following reason. It would be desirable to indicate clearly where the cloud was but this is difficult for semi-transparent cloud and the aircraft relative humidity and satellite IR radiance data are somewhat contradictory. In constructing the cloud boundaries greater reliance was placed on the IR radiance than the relative humidity: optimum interpolation tends to smooth out sharp gradients and therefore it was not appropriate to rely on the objective humidity analyses for placing the cloud edges. However the use of satellite data to delineate vertical extent is particularly difficult. The cloud edges for missions 207 and 208 were particularly hard to distinguish.

For missions 201 and 207 the vertical shear in the domain at the levels of interest was considerable: about 25 m/s in 100 hPa in the case of 207. Bearing in mind that each high resolution cross-section just fits within a 32 * 32 segment, the horizontal shear is significant for all missions except 207. (In this report the term segment always means a 32 * 32 array of IR pixels).That is to say, the horizontal shear across the segment approaches or exceeds 10 m/s, and therefore the error resulting from assuming that a wind, which may be representative of the motion in only part of the segment, is representative of motion centred on the middle of the segment, could be considerable.

It was considered desirable to place the high resolution cross-sections in the context of the complete jet stream, showing where the wind maximum was relative to the cirrus used to generate the winds in this study. In order to do this, low resolution cross-sections were also generated, covering the domain of the high resolution

section and the wind maximum, and these sections are shown in figures 3.2.1 to 3.2.4. These sections were generated using simply the background field, i.e. the operational analysis, so they are not necessarily consistent with the high resolution sections, which are strongly dependent on the aircraft data. The sections illustrate the point that the cirrus that was tracked was some way from the jet core in all except one case. However there may well have been more cirrus between that which was tracked, which was of neccessity in the ICE experimental area, and the jet core.

Generally speaking, the variability of wind speed with height contributes more to errors stemming from height assignment problems than does the variability of wind direction, and this is why wind speed was shown in the figures. However, in the next section wind hodographs are shown which give an indication of the variability of direction as well speed.

3.4 Cross-sections of wind and humidity from FRONTS87 experiment

It was considered to be of some interest to show some cross sections from dropsonde data obtained in the Mesoscale Frontal Dynamics Project/FRONTS87 experiment (Thorpe and Clough, 1991). Figures 3.3.1 and 3.3.2 show the along-front component of wind and the 90% relative humidity contour for IOPs 7 and 8 of that experiment. (IOP 7 took place on 9th January 1988 and IOP 8 on the 12th). In the absence of the 100% contour, the 90% contour can be taken to indicate the edge of the cloud. Indeed it is very rare for the sondes to register high humidities immediately on release from the aircraft, so it is quite feasible that the cloud in both cases extended vertically up to and above the level of the aircraft. What the figures show is that the horizontal shear in the cloud is as great as elsewhere, but the vertical shear is not as strong as that found in the frontal region on the cold side of the cloud. Note though that in FRONTS87, cold fronts were being examined and it is quite possible that in warm fronts the cloud is colocated with the zone of maximum vertical wind shear.

The horizontal and vertical scales of these cross sections are different to those of the ICE experiment. Also the contoured variable here is wind component, but in a frontal situation the variability of wind speed is dominated by the variability of the along-front component. The contours of along front velocity in the frontal region have a slope of about 1 in 60: this figure will be refered to in section 6.

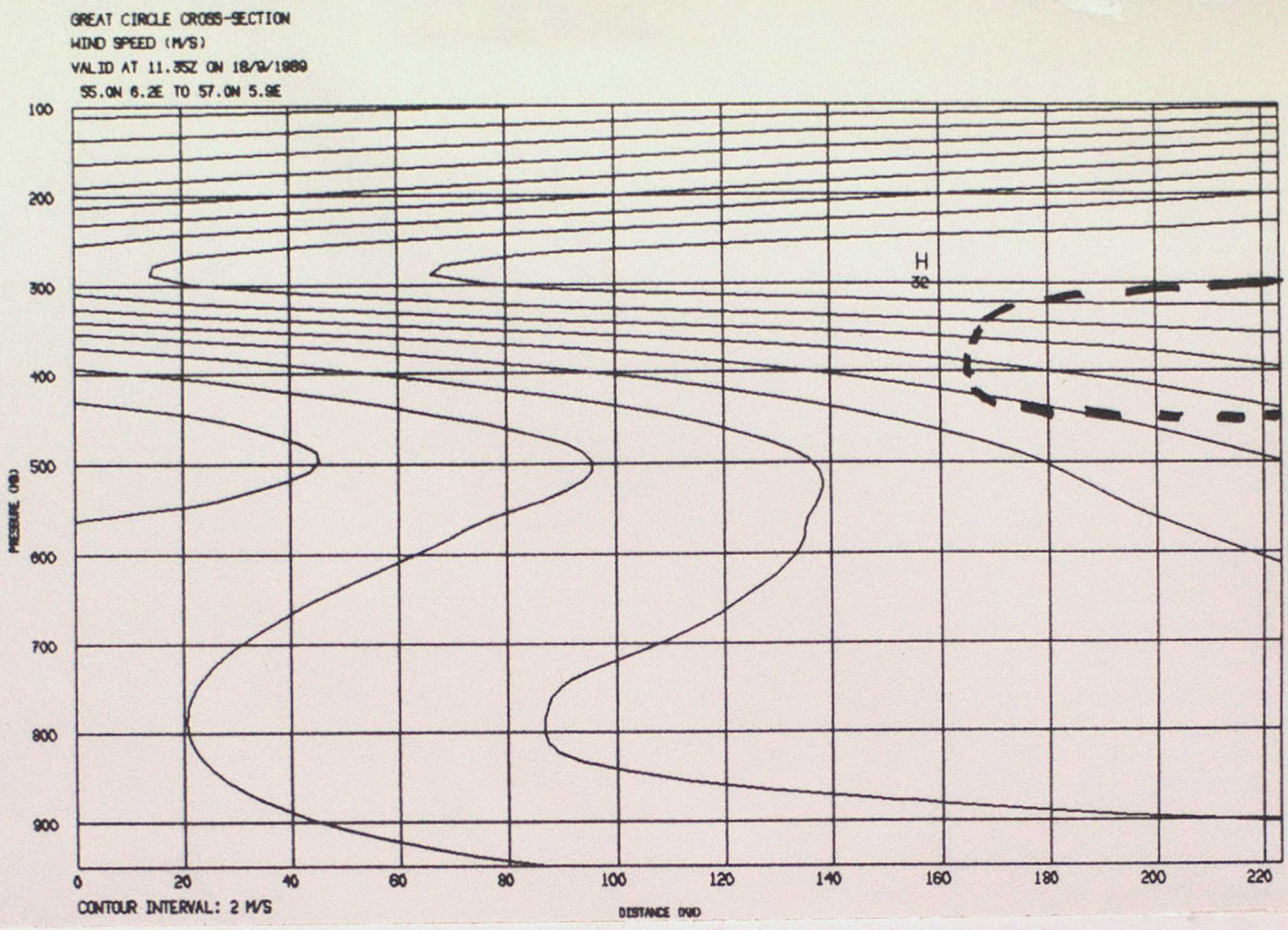

Figure 3.1.1 High resolution cross section of wind speed, plus approximate cloud boundary (thick dashed line) for ICE201

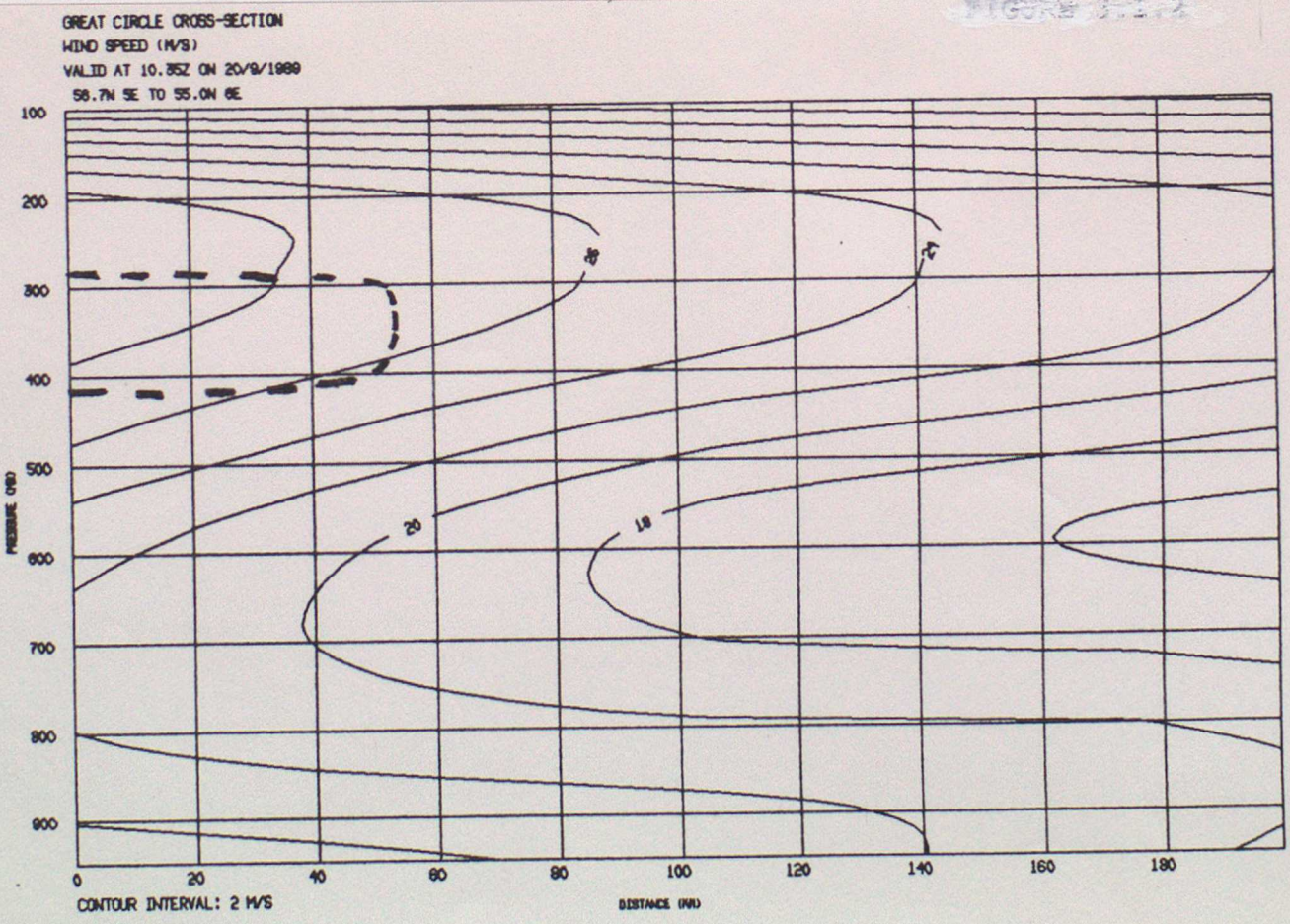

Figure 3.1.2 High resolution cross section of wind speed, plus approximate cloud boundary (thick dashed line) for ICE202

FIGURE 3.1.3

Figure 3.1.3 High resolution cross section of wind speed, plus approximate cloud boundary (thick dashed line) for ICE207

FIGURE 3.1.4

Figure 3.1.4 High resolution cross section of wind speed, plus approximate cloud boundary (thick dashed line) for ICE208

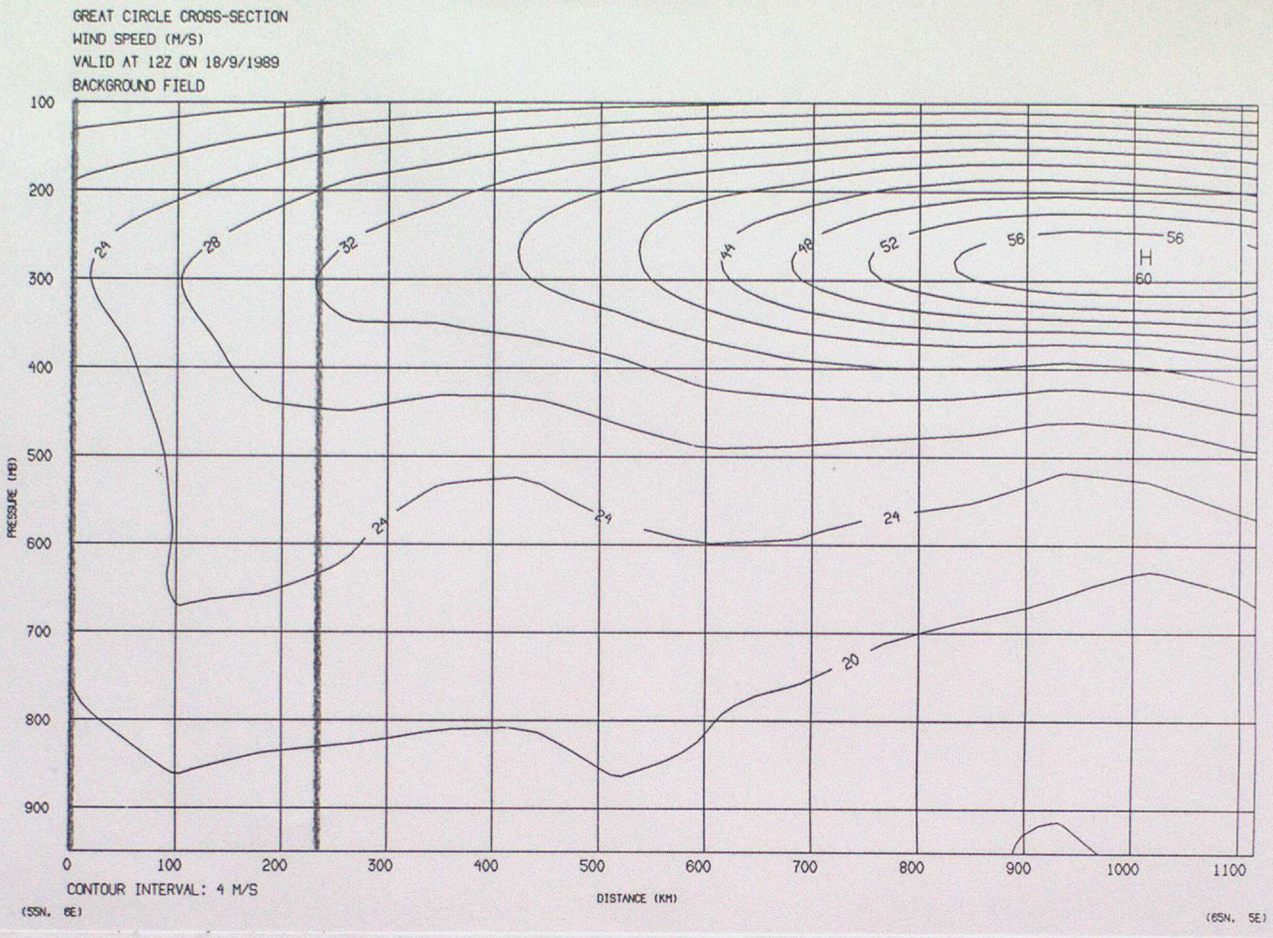

Figure 3.2.1 Low resolution cross section of wind speed for ICE201. Bold vertical lines indicate domain of high resolution section.

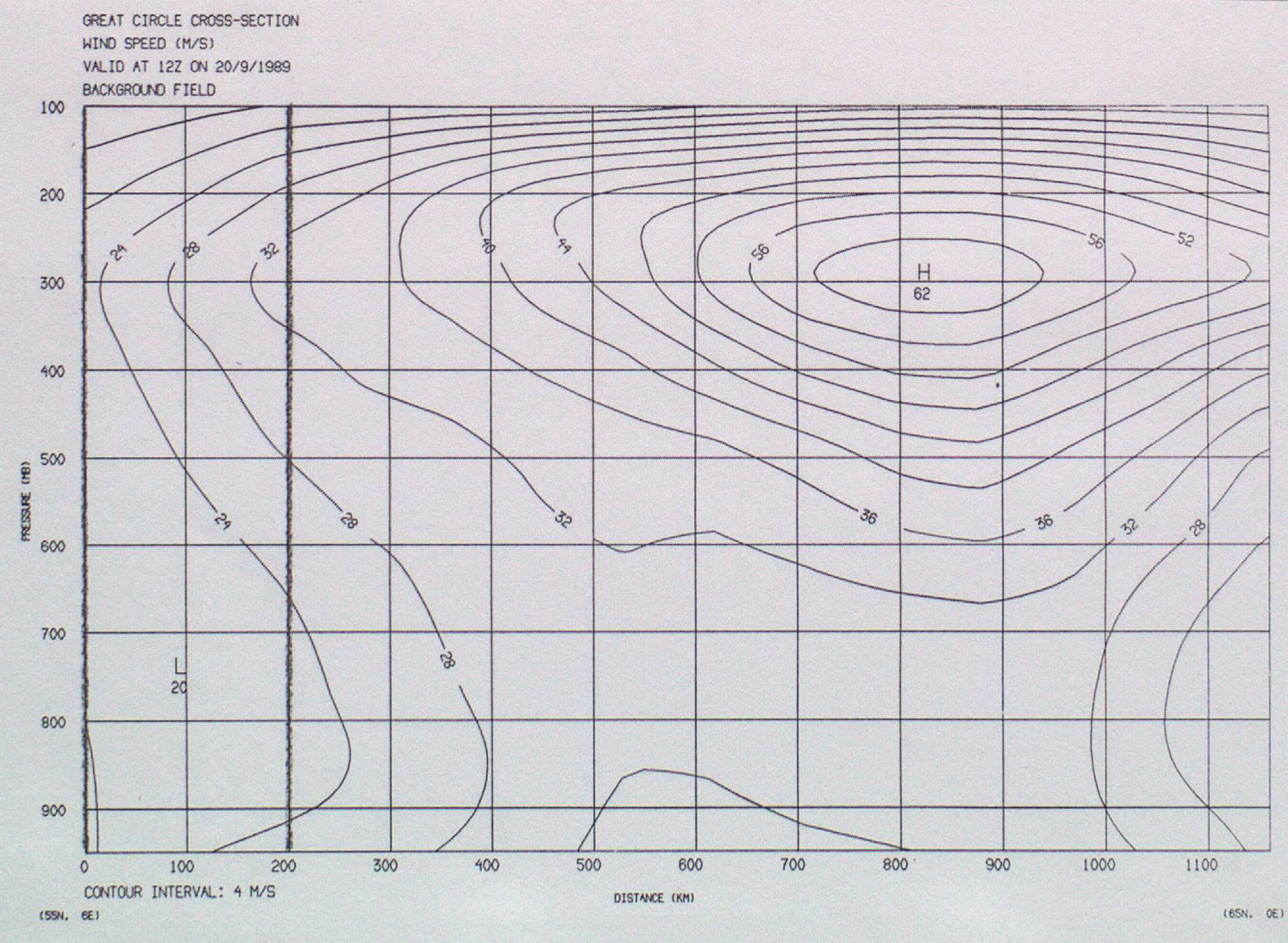

Figure 3.2.2 Low resolution cross section of wind speed for ICE202. Bold vertical lines indicate domain of high resolution section.

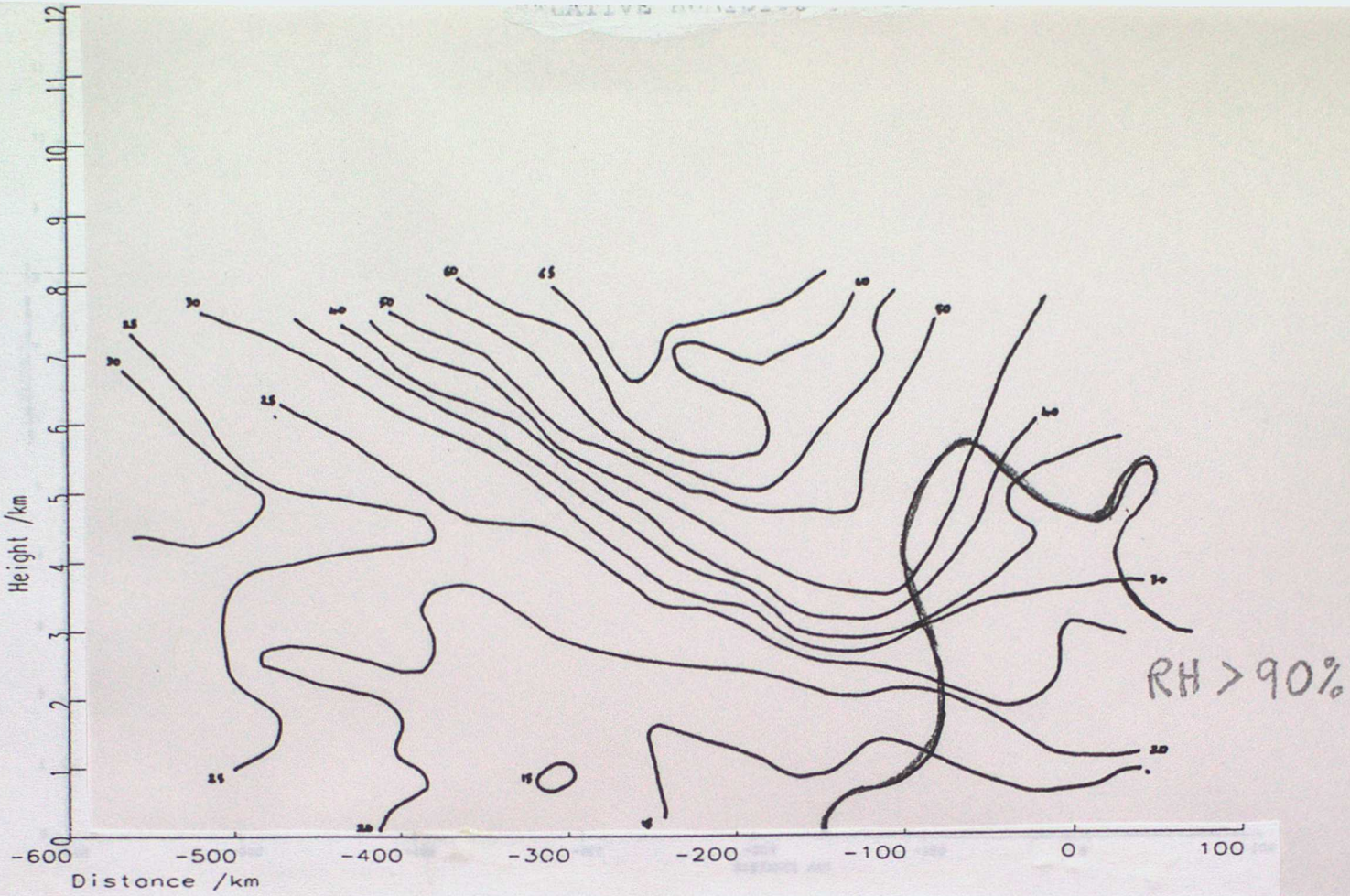

Figure 3.3.1 Cross section of along front velocity and 90% relative humidity contour for FRONTS87 IOP7

Figure 3.3.2 Cross section of along front velocity and 90% relative humidity contour for FRONTS87 IOP8

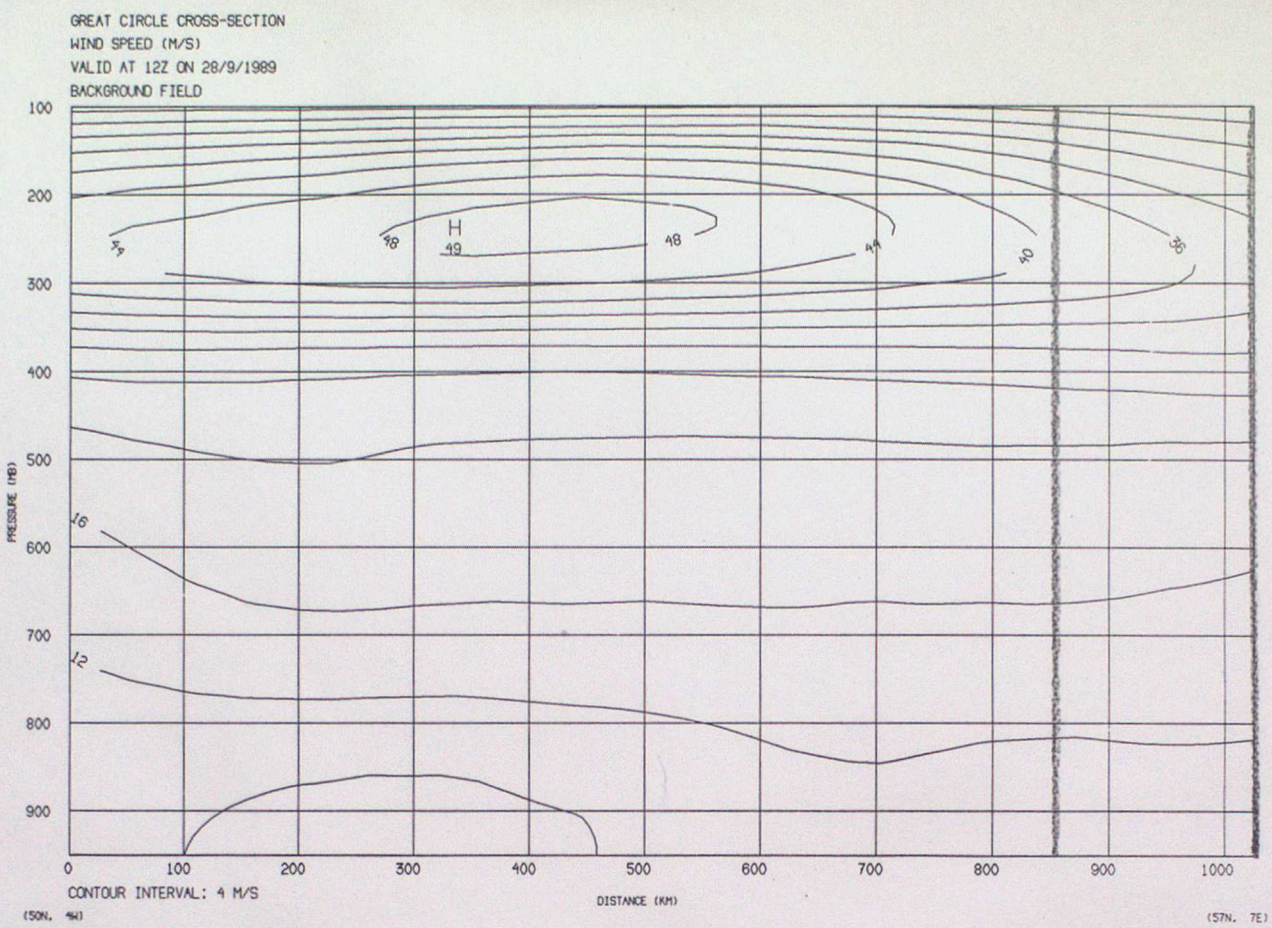

Figure 3.2.3 Low resolution cross section of wind speed for ICE207. Bold vertical lines indicate domain of high resolution section.

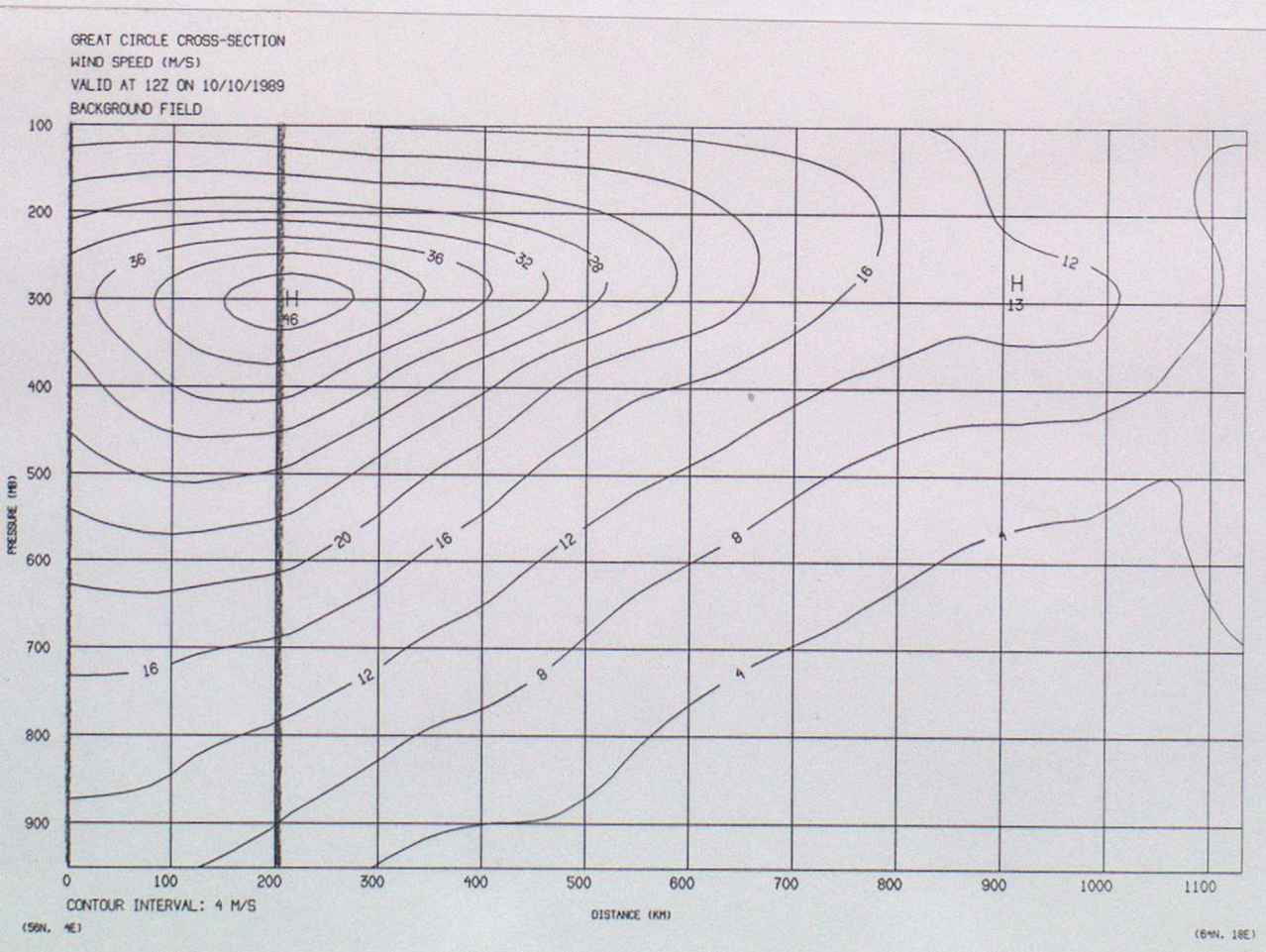

Figure 3.2.4 Low resolution cross section of wind speed for ICE208. Bold vertical lines indicate domain of high resolution section.

4 Comparison of cirrus motion with the actual wind on various scales

4.1 The method used to generate "correlation surfaces"

In general, the production of SCMWs by automated means relies on the calculation of the correlation between a pair of images at successive times, for a range of possible displacements of one image relative to the other. This two-dimensional array of correlations is generally referred to as a correlation surface. Although operationally at ESOC the true correlation coefficients are calculated, in the present study the Sequential Similarity Detection Algorithm (SSDA, Wilson, 1984) was used. SSDA is simply the sum of the magnitudes of the differences between the images at the specified displacements. Thus whereas one seeks maxima in true correlation surfaces as indications of the true wind, in SSDA surfaces one seeks minima.

One advantage of SSDA surfaces is that if one has already calculated them for two templates, say, two neighbouring 8 * 8 arrays, then in order to generate the one for the 16 * 8 template comprising the two original 8 * 8 templates, one simply adds the two existing surfaces. This property was exploited in the present work: altogether template sizes of 8*8, 8*16, 16*16, 16*32 and 32*32 pixels were all processed. (An 8*16 template has 8 pixels in the north-south direction and 16 pixels in the east-west: at the latitude of the North Sea this is roughly square on the earth's surface. The operational production of SCMWs uses a template size of $32 * 32$ infrared pixels, but Lunnon and Lowe (1992) showed that the use of a smaller template size produces better results for low level SCMWs. Because the term correlation surface is used throughout the SCMW literature, it will be used in this report but the algorithm actually used was SSDA.

The process of generating correlation surfaces involves firstly the construction and interpretation of the histogram of infra-red radiances in the relevant portion of the image. Radiances warmer than a specified threshold are considered to arise from the background and those pixels are "smeared" so that only motions in the relevant cloud layers are tracked. Smearing consists of setting all pixels whose radiance exceeds what is termed the infra-red threshold to a constant value, which is equal to the mean of the original radiances of all those pixels. The threshold was determined by visual inspection of the histograms: the values used are recorded in table 5.1 (see section 5). Correlation surfaces are then generated using the smeared images.

Consideration was given to the use of the spatial coherency method of filtering the effects of underlying clouds (Coakley and Bretherton, 1982). However this is believed to be most effective when there are at least three peaks in the IR histogram, and as the histograms shown in section 2 indicate, this was not the case for the selected missions.

In producing correlation surfaces, unrectified images were used and the deformation information processed to provide the correction in position at the centre of the segment being processed. If images which have been rectified on a nearest neighbour basis are used, it can be shown that the ommision or repetition of lines (or columns) of data can lead to significant tracking errors. However, in our processing the sub-pixel part of the deformation information was ignored, and this may lead to errors. Noting that the RMS error in rectification at the time was about 1 to 2 IR pixels (Diekmann and Amans, 1990), it is not clear that there is useful information in the sub-pixel part of the deformation information. However the rate of change of rectification error may be quite small, and it is this which is significant for SCMW extraction.

Before comparing the analysed aircraft wind data with the correlation surfaces, the former were averaged onto the spatial scale of the latter, which is of course a function of the template size. Having produced the correlation surface, the next stage is to produce an empirical level of best fit (ELBF) - this is the level at which the CMW agrees best with the aircraft data. This is described in the next section. Of course an ELBF will be produced for each correlation surface at each scale.

4.2 On the derivation of empirical levels of best fit (ELBFs) for SCMWs

It is generally accepted that the major source of error in upper-level SCMWs is the combined effects of the height attribution error of the cloud being tracked and the fact that cloud motion may not be representative of the wind at the cloud top. These two theoretically separable sources of error can be very difficult to separate in practice unless there is clear in situ evidence for the height of the cloud, which for thin cirrus is rarely the case. In any case, what the user wants is a wind together with a height at which it can be considered representative, so the exact height of the cloud top may be irrelevant. What is needed is that any scheme for height assignment is tuned to produce a height which agrees closely with the empirical level of best fit (ELBF), defined conceptually to be the level in the atmosphere at which an SCMW agrees best with a complete profile of winds, irrespective of any height derived from the radiances from which the wind itself was derived. Thus great care needs to be taken in the derivation of the ELBF, because an erroneous ELBF will give rise to an inappropriate tuning. Although height attribution/unrepresentative motion of the cloud is the dominant

source of error in SCMWs it is not the only source of error, and if the other sources of error are ignored then clearly the ELBF might be misleading.

One possible such error is a conjectured speed bias in the SCMWs. However, given the vertical wind shear in the atmosphere, it can be argued that a plausible cause of any speed bias is erroneous height attribution, so it would be incorrect to make any allowance for a speed bias before calculating the ELBF. In fact it is argued that an apparent speed bias in SCMWs is in fact an artefact of the data used to verify the SCMWs. It was shown in Lunnon and Lowe (1991) that if numerical model data are averaged (vectorially) onto the scale of the SCMW, there is negligible speed bias: furthermore it should be remembered that operationally produced SCMWs relate to time intervals of 1 hour, on which mean wind speeds are lower than the conventionally used time interval of 10 minutes. Before SCMWs are compared wih the aircraft data obtained in the ICE experiment, the latter are averaged onto the spatial scale of the former, so it is considered that the speeds of the SCMW and the aircraft data are directly comparable.

In assigning an ELBF, it is natural that more weight is given to the component of wind having the greater vertical shear than the orthogonal component. Indeed, if the ELBF were calculated by simply dropping a perpendicular in the wind hodogram from the SCMW to the profile of the aircraft data, then no weight is given to the component having no shear. However, geometrical operations on a hodogram have to be considered carefully because such operations could be dependent on the coordinate system used to construct the hodogram. The concept of dropping a perpendicular is exactly equivalent to finding the point on the profile such that the sum of the squares of the x- and y- components of the distance from the SCMW is minimised. Hence if one scale was changed independently of the other, one would not derive the same ELBF. This is illustrated in figure 4.1, which is also used to make further points in the description of our derivation of the ELBF. In figure 4.1 S is the SCMW, and AB is a straight line representing the profile of winds. It is reasonably clear that in the projection as displayed, the point P is the nearest point on the line to S, i.e. P is the foot of the perpendicular from S to the line. However, if weights are given to the two components of wind as indicated by the scales designated by the figures in the diagram, the point Q is the "nearest" point on the line to S. This arises because a certain geometric distance in the y direction on the diagram is given lower weight than the same geometric distance in the x direction.

Some justification needs to be provided for considering such different projections of the hodogram. It is simply that in the area where the ICE experiment measurements were made, a METEOSAT pixel has an aspect ratio of slightly more than two, that is, the separation of lines of pixels in the north-south direction on the ground is more than twice the separation of pixels of the same channel in the east-west direction on the ground. Thus if one generated an ELBF by dropping a perpendicular in space-view coordinates one would get a significantly different answer from that obtained using a conformal projection, and it is unclear which of these two solutions is to be preferred. Admittedly, in Figure 4.1 the x- and y- scales have a ratio of about 2.4, but this figure should be regarded as being illustrative of the effect.

Another factor that should be taken into consideration when constructing ELBFs is that, quite apart from errors arising from height attribution, the error in one component of the SCMW might be greater than the error in the other. The most likely cause of this would be if features in an image were quasi one-dimensional, then determining the component of wind parallel to the cloud edge would be rather difficult. In such circumstances it would clearly be inappropriate to give much weight to that component in calculating the ELBF. Thus ideally one would like not simply a single SCMW but a range of possible values with probabilities (or, conversely, likely errors) attached to each value. It is recognised that sources of error such as image navigation are likely to be anisotropic (for example,if navigation was performed by reference to coastline, and in a particular area the coastline was very straight, then one component of the navigation error would be likely to be bigger than the other), but this is difficult to quantify. Thus we assume that the sources of anisotropy in the error in the SCMW aside from the height attribution are dominated by the tracking error, which we can quantify by examination of the correlation surface. This is the justification for our working definition of the ELBF that it is the point on the wind profile which has minimum SSDA (which is equivalent to the point having maximum correlation). Point R on Figure 4.1 is that point: the continuous lines on Figure 4.1 are contours of the correlation surface. It will be noted that it is a different point from either P or Q. The particular virtue of this definition of the ELBF is that it is independant of the coordinate system used to specify the hodogram, obviating the ambiguity between P and Q that arose through different projections.

Given the variability of both correlation surfaces and vertical wind shear, it is clearly essential to have a quantitative indicator of how reliable an ELBF is, i.e. what is the likely error in it. Given the working

definition of ELBF given above, the obvious quantity to use is the second derivative of correlation with respect to pressure **following the wind profile**. In the diagrams that follow this quantity is designated by the term D2CDP2. Thus D2CDP2 takes into consideration both the vertical wind shear (which is a vector, of course) and the sharpness of the peak in the correlation surface (which is also a vector).

It is worth commenting that although the data used to construct Figure 4.1 were hypothetical, the scenario of correlation surface and vertical wind shear implied by this figure is eminently plausible, in frontal cases. The symmetry of the imagery is likely to give rise to an elliptical correlation surface, with the semi-major axis of the ellipse parallel to the front. The wind shear in a front is also likely to be approximately parallel to the front.

4.3 Examples of real correlation surfaces and aircraft wind profiles

Figure 4.2.1 shows information analagous to figure 4.1, i.e. the correlation surface, the vertical wind profile obtained from the aircraft data, the ELBF and in addition the level obtained from implementing the semi-transparency correction. The method used to obtain this is discussed fully in section 5: at this stage it should be recorded that the WV channel calibration coefficient used was 0.0065 $WM^{-2}St^{-1}Ct^{-1}$. Figure 4.2.1 is for a template size of 32*32 pixels (which we denote for convenience as scale 5) for 1135GMT for mission 201 (note that a doublet of images is used, for which the image times over the North Sea are approximately 1120GMT and 1150GMT). The nomenclature for different different template sizes, which will be used in the following sections, is that a template size of 8 * 8 is scale 1, 8 * 16 is scale 2 and so on, with 32 * 32 being scale 5.

The correlation surface contours are continuous, while the wind profile is dashed and letters are used to designate specific points on it. The key to the letters is shown at the top left of the figure. The figure adjacent to the pressure levels indicate the error levels in the aircraft data. A value of zero indicates that there were a number of aircraft observations made use of in the analysis at that point in space/time, whereas a value of unity indicates that the analysed field simply reproduces the background field. However the background field is itself an analysis of the operationally available data. There are two figures for each level, the first pertaining to the u (east-west) component, the second to the v (north-south) component. The figures are different because although the covariance functions in terms of velocity potential and stream function are isotropic, in terms of wind components they are not.

The other data shown in figure 4.2.1 are as follows. CDOTOP and RDOTOP are the optimum (i.e. level of best fit) values of CDOT and RDOT, which are the x and y components of velocity in space-view coordinates (the C relates to column number and the R to row number). Note that these coordinates are used in the diagrams themselves, in which the units are infra-red pixels per half hour: in converting to, for example, knots, it should be born in mind that an infra-red pixel is approximately 5km by 10km at these latitudes. Thus a CDOT of 1 infra-red pixel per half hour is approximately 10km/hour, i.e. approximately 5.4 knots, whereas an RDOT of 1 infra-red pixel per half hour is approximately 20km per hour, i.e. approximately 10.8 knots.

CMIN denotes the value of SSDA at the ELBF, and PMIN is the pressure of the ELBF. On the figure itself the level of best fit is denoted by a star. An S is used to denote the wind at the level which the semi-transparency correction gives as the level of the cloud. As discussed earlier, D2CDP2 is the second derivative of SSDA as a function of pressure.

In this example the wind profile passes encouragingly close to the minimum in the correlation surface, and the empirical level of best fit (334.4mb) is in passable agreement with the pressure derived from the semi-transparency correction (approximately 400mb). For other scales and times the situation is not so good.

Figures 4.2.2, 4.2.3 and 4.2.4 are examples analagous to figure 4.2.1 for the later missions (numbering convention as in section 2). They are all for scale 3, i.e. template size of 16 * 16 pixels. Figure 4.2.2 illustrates the fact that at this scale, the correlation surfaces are not as smooth as at larger scales, but the aircraft data clearly identify the correct peak. However the wind profile is such that finding the ELBF is very sensitive to the precise position of the peak. In practice the ELBF used subsequently was found by excluding aircraft data except between 500mb and 250mb: in this way the ambiguity was removed. This difficulty is also apparent in figure 4.2.3, although at least for this case there is only one peak in the correlation surface. Note how anisotropic the correlation surface is and the fact that the vertical wind shear is approximately parallel to the axis of maximum uncertainty, as forseen in figure 4.1. In figure 4.2.4 the correlation surface does not have such a sharp peak as is found for the other missions, and this is brought out in the D2CDP2 figures, which are also listed in section 5.

4.4 The generation of winds from correlation surfaces

Provided there is only one peak in the correlation surface, generating the wind is straightforward. This of course depends on the size of search area. In general it is possible to get away with a fairly small search

area by using a numerical forecast to indicate where in displacement space the search area should be. For the processing of I.C.E. data, manual intervention was allowed to select an appropriate search area.

Although there is frequently only one peak in the search area when a 32 * 32 template is used, for smaller templates the correlation surfaces are more noisy, and there can be spurious peaks. The following approach was used to discriminate the correct peak. In choosing the peak at each scale, the search was started at the location of the peak in the next larger scale. The justification for this strategy is as follows. It is reasonable to suppose that, for adjacent templates of the same size, the true peaks must lie in approximately the same part of the search areas (otherwise the winds that result will exhibit unrealistic small scale variability). Furthermore, if there are such peaks for two neighbouring small templates then there will be a peak for the larger template that exactly comprises the two small templates, and that peak will correspond to a wind which is close to those corresponding to the peaks for the smaller templates.

Having found the peak in the correlation surface, the sub-pixel movement is found by fitting a bi-quadratic surface, as is done operationally at ESOC.

4.5 Examples of winds at various scales

Figures 4.3 show examples of wind produced for relatively small scales from the various missions (numbering convention as previously). Figure 4.3.1 shows winds for scale 1, which has a template size of 8 * 8 pixels. Although the variation in direction is plausible, the variation in speed is not. However, in figure 4.3.2, which is for scale 2 (8 * 16 pixels) the variations of both speed and direction seem eminently reasonable. In figure 4.3.3, the sense of the variations in speed and direction are plausible, but the magnitude of the variations are perhaps too great. This can probably also be said for figure 4.3.4. In conclusion we can say that there is no evidence of plausible variations on the scale of the individual winds portrayed, but there is clear evidence that there are gradients in the wind which would be successfully resolved by the use of a 16 * 16 template.

4.6 Summary statistics of agreement between SCMWs and aircraft data on various scales

In order to assess quantitatively, but without reference to any height attribution process, the extent to which cloud motions are representative of the true wind field, statistics were generated as to the accuracy of winds at the ELBF. However, it was recognised that for the smallest scale winds, the ELBF might be misleading in the sense that noise in the SCMWs could be accomodated by using a slightly erroneous height attribution. Therefore, not only was the ELBF at the scale in question used, but in addition the winds were verified using the ELBF from the 32 * 32 scale. Verification was performed by comparing the wind using the prescribed height assignment with the wind derived from the aircraft wind at that level, and the root mean square vector difference was calculated. The results are given in the following table (RMS vector differences in pixels per half hour). The results are for all the missions and times specified in table 5.1.

Scale of wind	$8*8$	$8*16$	$16*16$	$16*32$	$32*32$	$8*8$	$8*16$	$16*16$	$16*32$
Scale of ELBF	$32*32$	$32*32$	$32*32$	$32*32$	$32*32$	$8*8$	$8*16$	$16*16$	$16*32$
RMS Vector error	2.67	2.40	1.94	1.56	1.55	1.88	1.56	1.81	1.48
No of cases	125	75	45	24	16	125	75	45	24

It had been hoped that there would be a single minimum in the statistics as a function of scale, with values increasing as a function of difference of scale from the optimum. Therefore it is difficult to explain the relatively high value for the 16 * 16 scale, using the ELBF at that scale for height assignment, which is considered to be anomalous. There is clear evidence that 16 * 32 is to be preferred to 32 * 32.

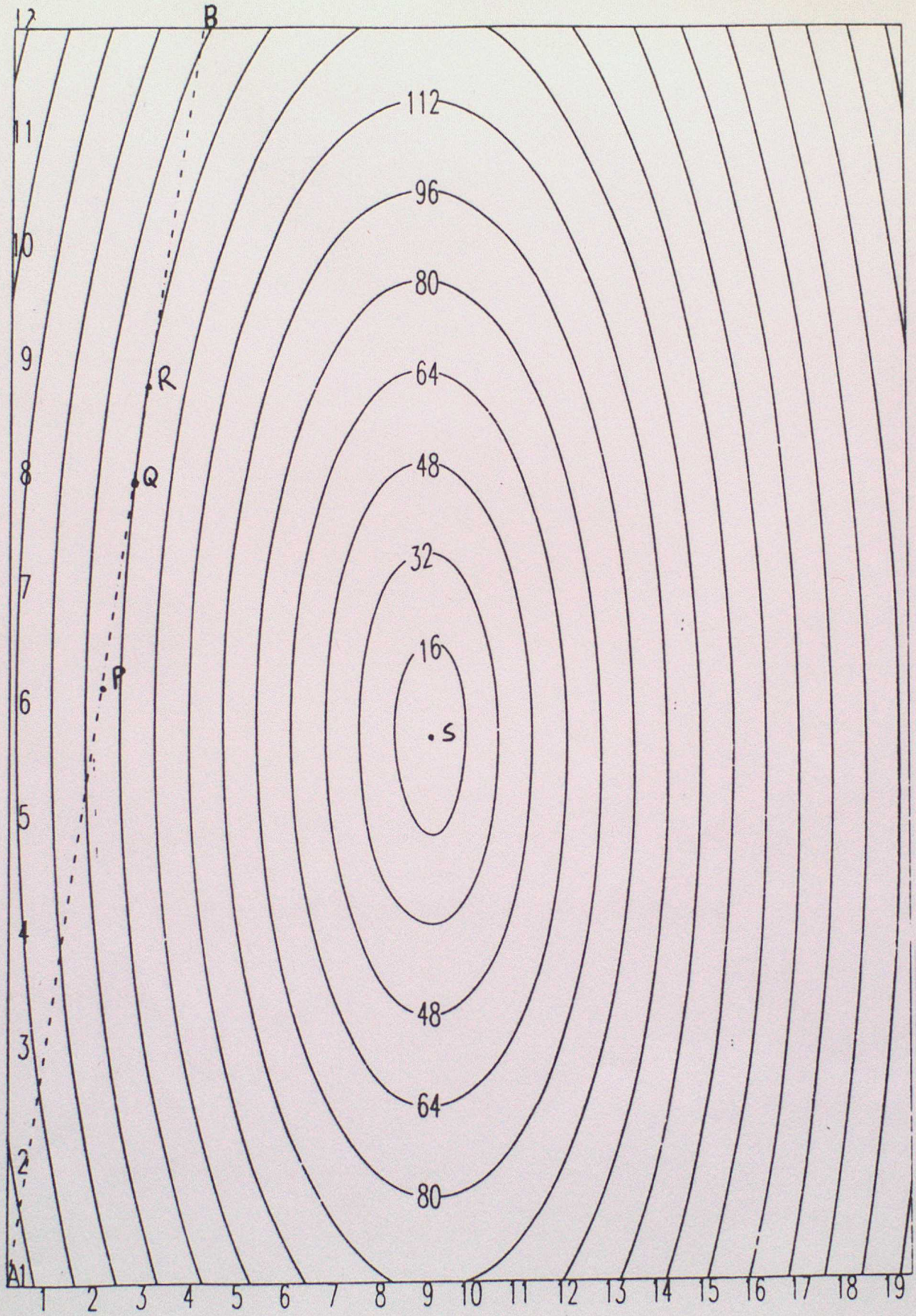

FIGURE 4.1 ILLUSTRATES IDEALISED CORRELATION SURFACE AND WIND HODOGRAM

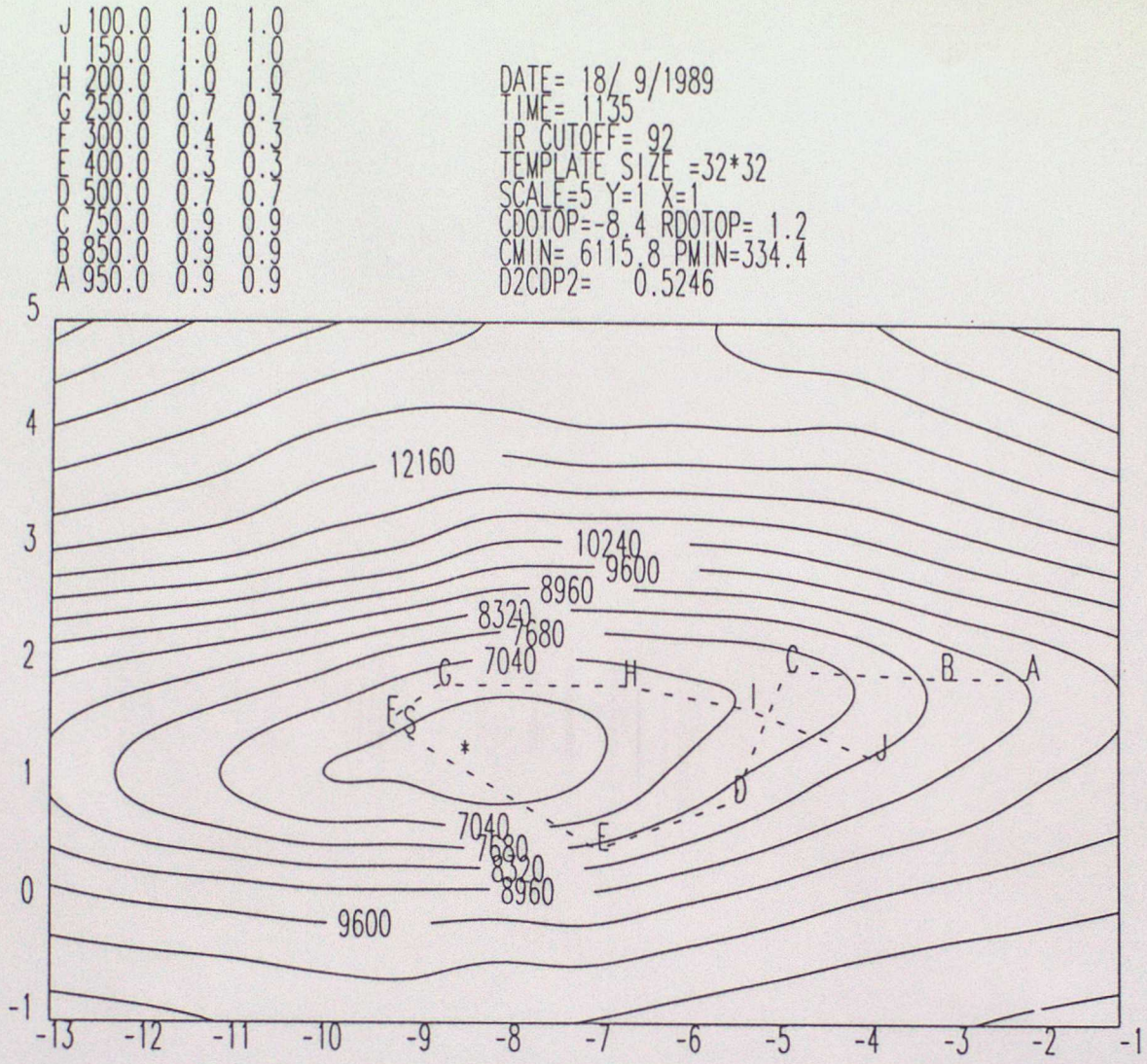

Figure 4.2.1 Example of "correlation surface" and wind hodogram for ICE201

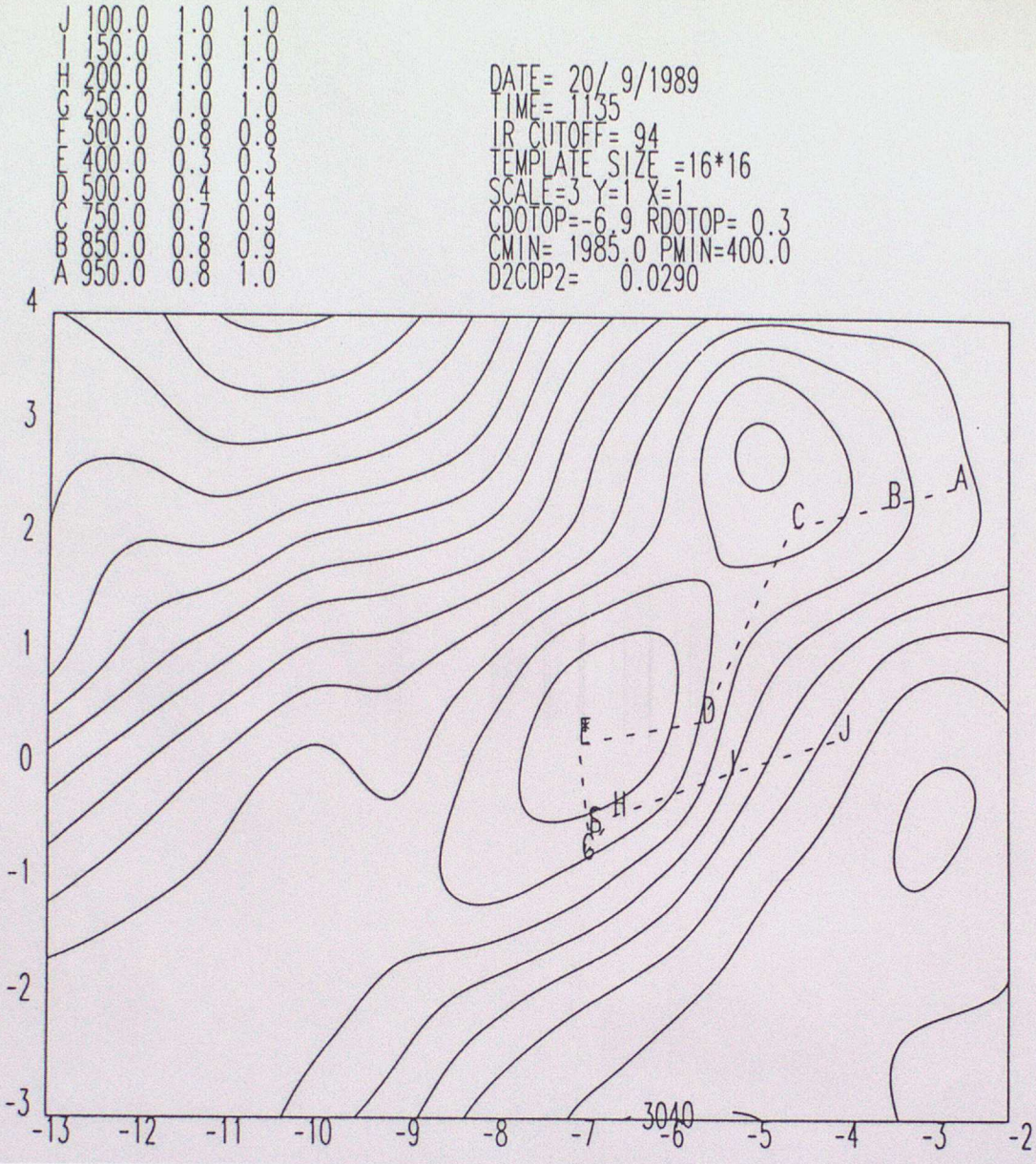

Figure 4.2.2 Example of "correlation surface" and wind hodogram for ICE202

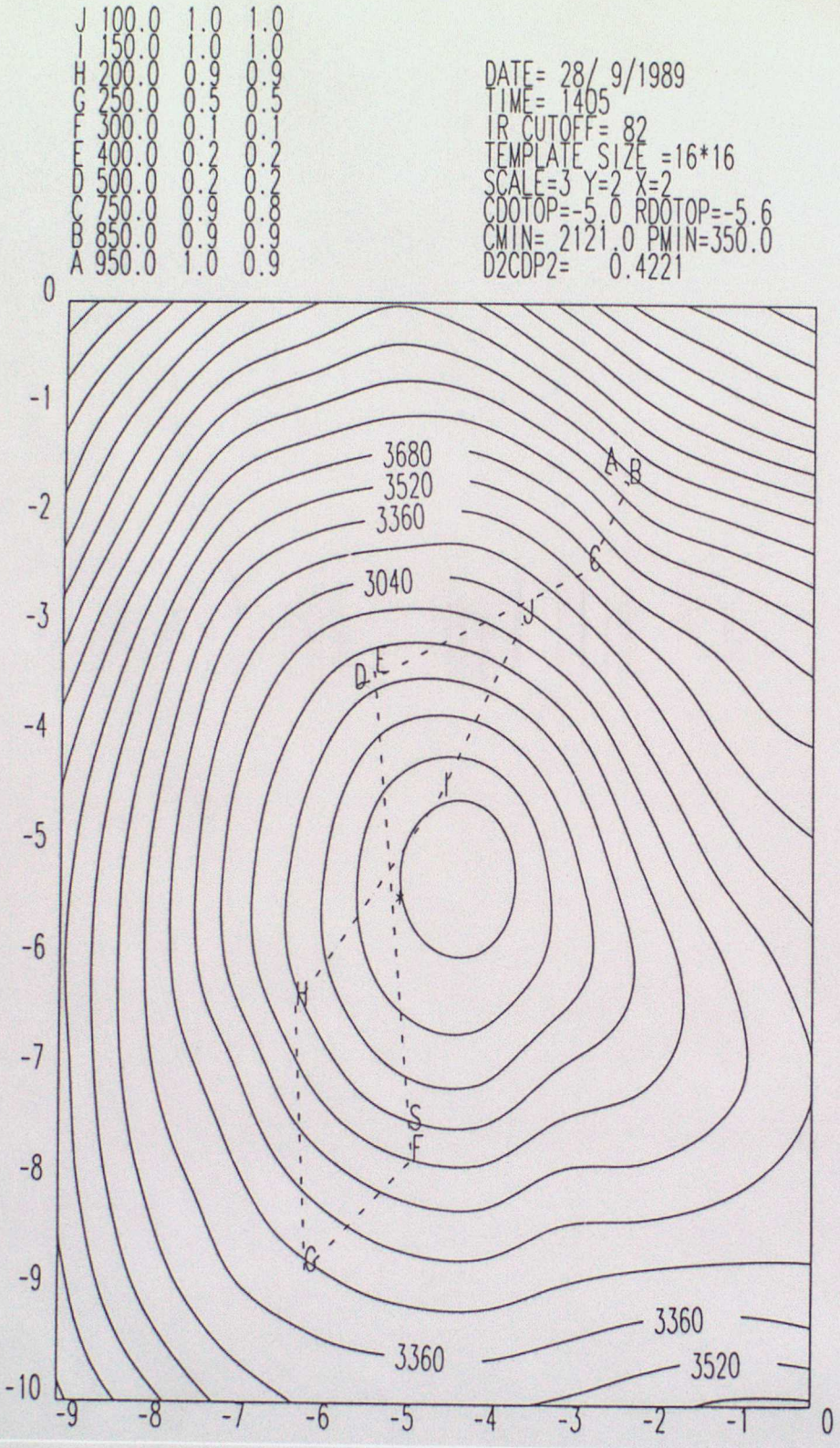

Figure 4.2.3 Example of "correlation surface" and wind hodogram for ICE207

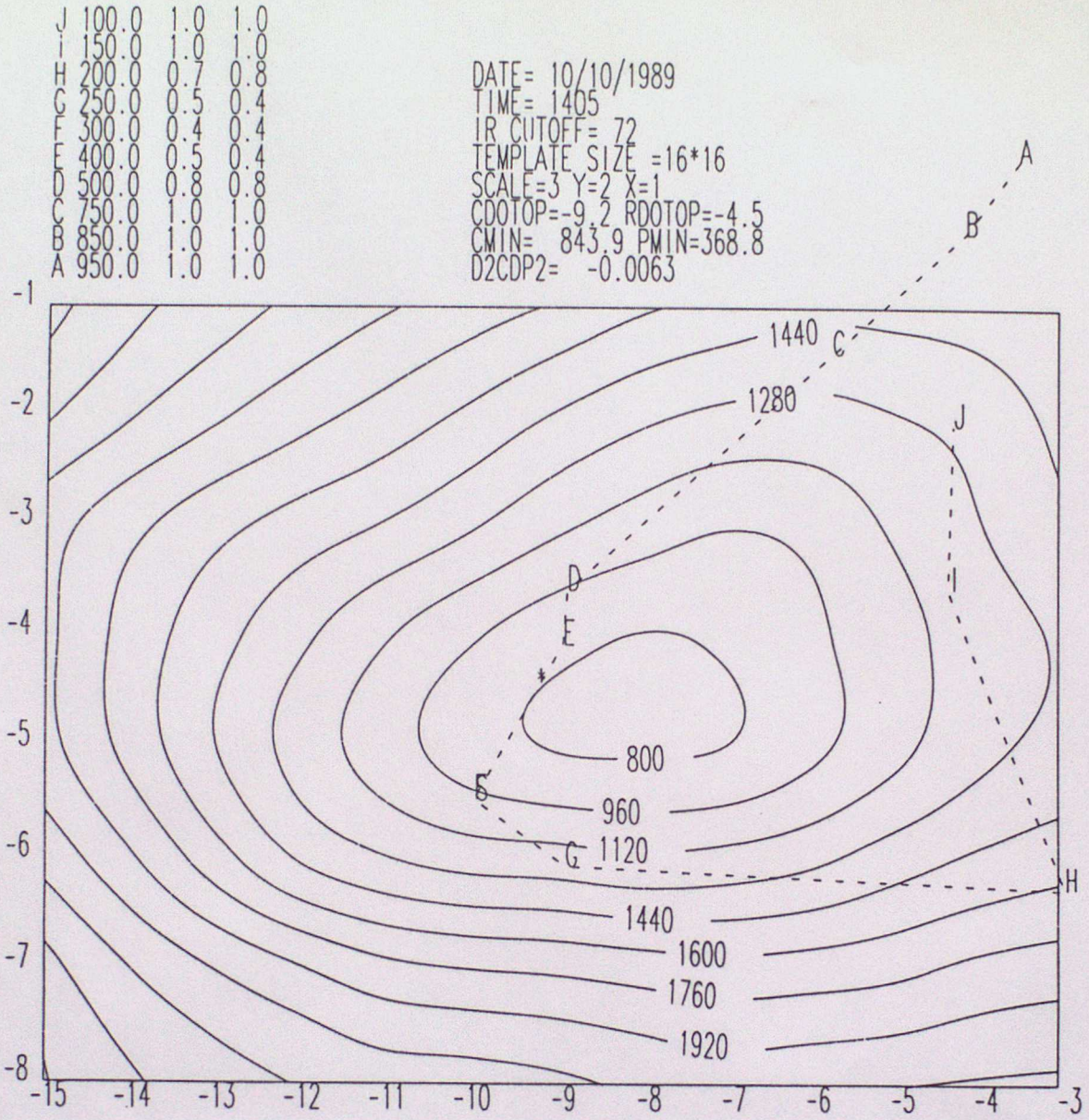

Figure 4.2.4 Example of "correlation surface" and wind hodogram for ICE208

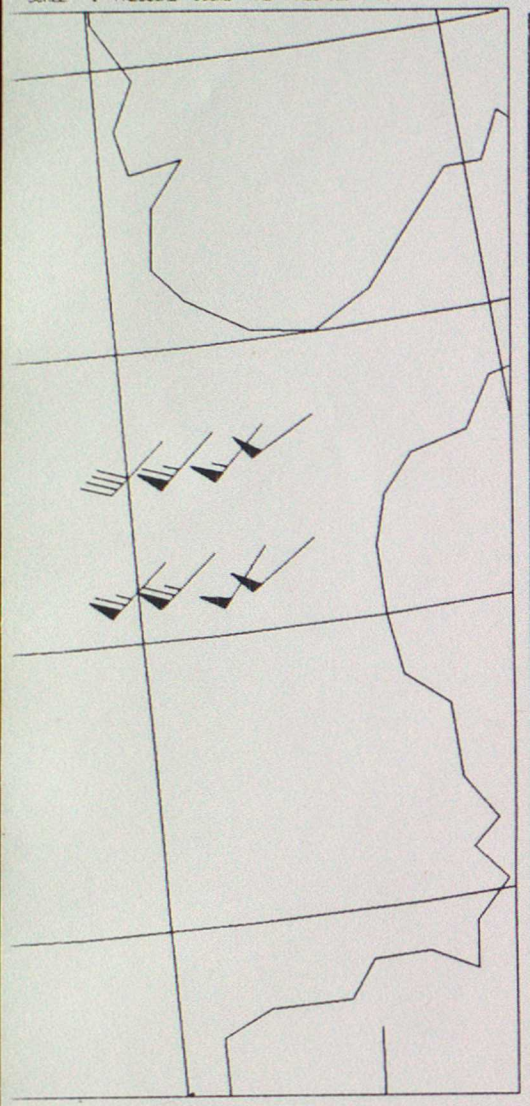

FIGURE 4.3.1

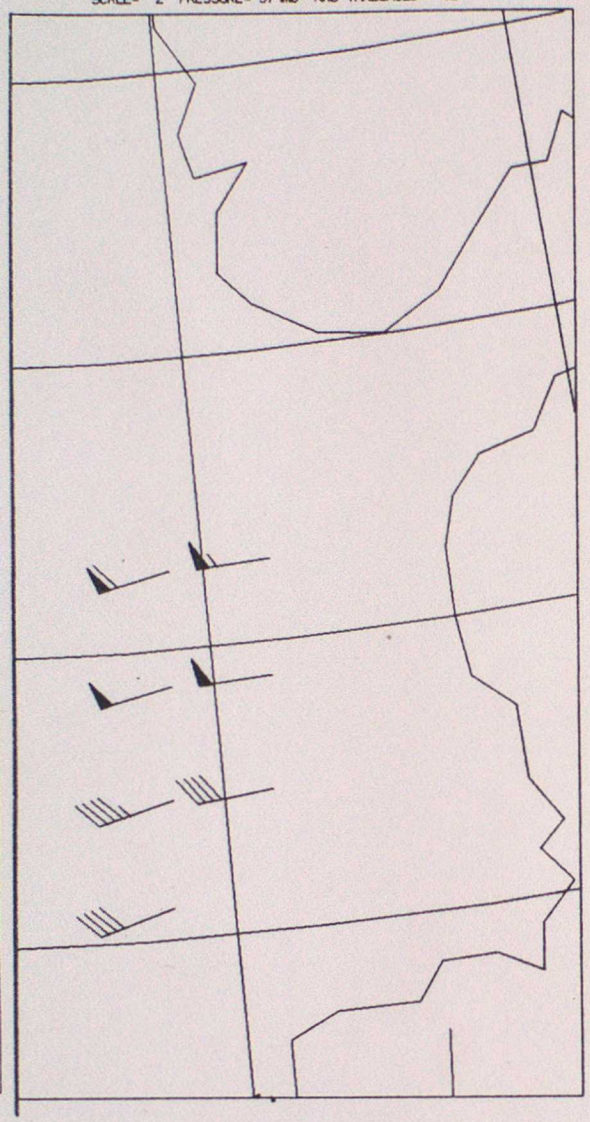

FIGURE 4.3.2

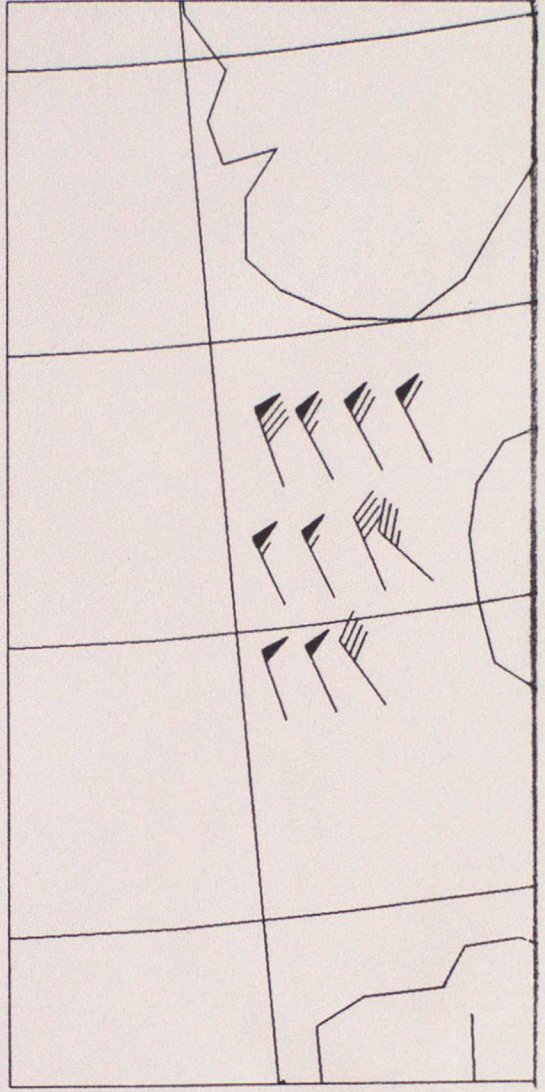

FIGURE 4.3.3

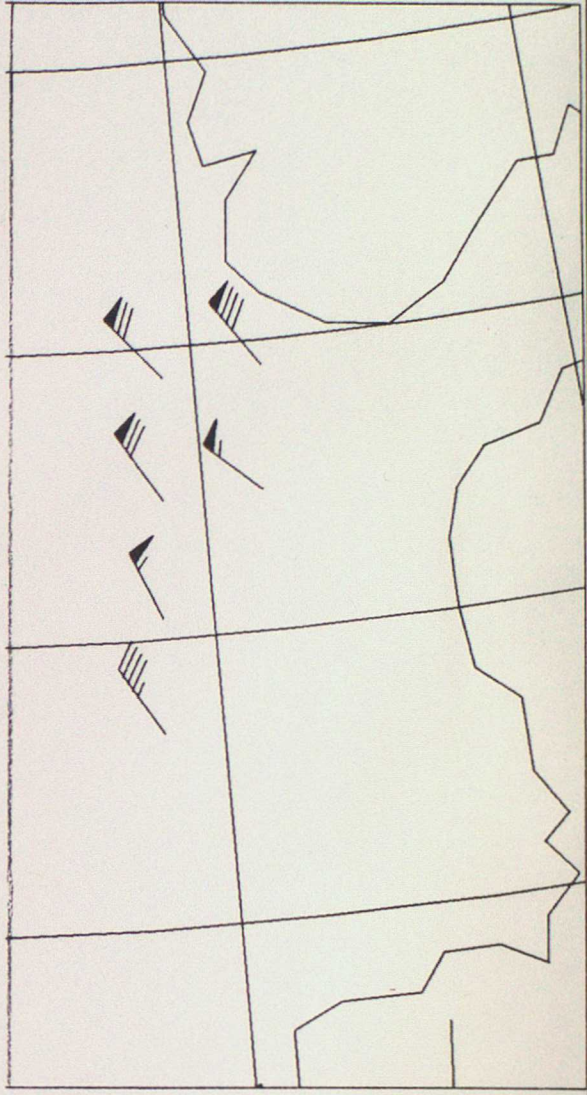

FIGURE 4.3.4

EXAMPLES OF CMWS PRODUCED AT SMALL SCALES

5 Application of the operational semi-transparency correction to I.C.E. data

5.1 Experience using the MIEC water vapour calibration

The calculation of the semi-transparency correction is performed exactly as it is done operationally at ESOC, as described by Bowen and Saunders (1984). However, the generation and selection of the model atmospheres for which the radiative transfer calculations are performed is different, and this is described in the appendix. Note that the model selection is performed using the aircraft data averaged onto the appropriate scale.

Briefly, the method consists of finding the intersection between two lines plotted in IR/WV radiance space. One line, referred to henceforth as the straight line, is a straight line connecting the cluster means for the background and cloud clusters. It has to be extrapolated to intersect the other line. This latter line is known as the opaque cloud curve, and it is generated using radiative transfer theory and a specified temperature and humidity distribution. It specifies what radiances would be observed at spacecraft level if an opaque cloud were placed at a variety of levels in the atmosphere.

The application of the semi-transparency correction is very sensitive to the registration of the WV and IR channels. Registration information is available with the archived image information obtained from ESOC, but using this alogorithm (admittedly, with the registration only applied to the nearest pixel) gave rise to occasions when the mean WV channel radiance for the background cluster was colder than the mean WV channel radiance for the cloud cluster. Therefore an empirical reregistration was applied whereby a total of 9 possible registrations were used (a 3*3 array centred on the ESOC registration) were examined, and the one that gave the minimum number of occurences of the background cluster being colder than the cloud cluster was used. This procedure was applied to arrays of 8*8 pixels, but a consistent registration was applied across the full segment of 32 * 32 pixels.

It was found that no semi-transparency correction correction was applied on a large number of occasions, because, given the infra-red radiance, the water vapour channel radiance is greater than the corresponding value on the opaque cloud line. There are a number of possible explanations of this, which will be considered in detail later in this section.

5.2 Vicarious calibration of WV channel

Because of the good measures of the ELBF obtained as described in the previous section, it was decided to use them to perform a vicarious calibration of the water-vapour channel, using the following steps:

1. Convert ELBF from pressure to temperature, using aircraft temperature data.
2. Convert temperature to infra-red black-body radiance in physical units
3. Convert I-R radiance to counts using published MIEC calibration coefficient
4. Use straight line of semi-transparency correction to give W-V radiance in counts (this process does not make use of any model atmosphere).
5. Use model atmosphere, specified in physical units, to give W-V radiance (in physical units) corresponding to I-R radiance (in physical units) from step 2.
6. Use two forms of W-V channel radiance, from steps 4 and 5, to give calibration coefficient.

The results are given in the table 5.1, which requires a little explanation. In addition to the mission number and time, the table gives the infra-red cut-off, used to discriminate between cloud pixels and background pixels, the mean, uncorrected radiances from the background and cloud clusters, the pressure of the ELBF and the radiance in counts corresponding to it, the vicarious calibration coefficient in $WM^{-2}St^{-1}Ct^{-1}$, the model atmosphere used (see appendix for the explanation of this number), the second derivative of correlation with respect to pressure, and the average visible channel variance for pixel pairs comprising infra-red pixels. (Note that from the archive, only every alternate line of visible data is available). A convention was adopted whereby if the radiance in counts corresponding to the ELBF is **higher** than the uncorrected radiance, the water vapour channel calibration coefficient was set to be negative. There is a perfectly reasonable explanation for this: it would occur if the cloud were opaque and moved with a wind at a level below cloud top. It is noteworthy that all the occurences of the ELBF being below (in the atmosphere) the level corresponding to the uncorrected IR radiance have rather low values of d^2c/dp^2, that is, there is considerable uncertainty about the ELBF.

Table 5.1

Mission /Time	*IR cut −off*	*IR B/G*	*IR cloud*	*IR ELBF*	*Press ELBF*	*WV Cal Coef*	*WV B/G*	*WV cloud*	*Model*	d^2c/dp^2	*VIS dif*
2011105	90	123	82	64	318	.0049	92	89	18	0.2	2.7
2011135	92	135	83	68	334	.0051	94	88	17	0.5	2.3
2011205	92	134	84	49	250	.0046	94	87	1	0.1	2.3
2021035	92	122	76	60	300	.0059	81	75	43	0.0	4.4
2021105	90	123	77	85	400	−.0049	80	76	43	0.0	4.7
2021135	94	124	82	60	300	.0057	81	71	43	0.0	4.6
2021205	96	128	87	90	430	−.0054	81	82	43	0.2	4.2
2071235	88	108	77	53	315	.0059	84	75	64	1.5	2.7
2071305	92	110	82	65	375	.0061	85	78	64	1.0	3.0
2071335	96	113	86	62	359	.0057	85	81	43	0.8	3.5
2071405	82	110	71	60	347	.0061	85	74	43	0.5	2.6
2081235	62	90	54	68	400	−.0070	71	61	64	0.0	0.8
2081305	72	90	59	68	400	−.0069	71	64	64	0.2	1.1
2081335	70	81	61	64	382	−.0069	68	65	64	0.1	1.2
2081405	72	80	65	68	400	−.0068	70	66	64	0.1	1.4
2081435	76	84	68	68	400	−.0068	72	67	64	0.1	1.6

Although the inconsistency between values of WV calibration coefficient is dissapointing, (and this variability will be discussed later) it is considered that a value of about 0.006 $WM^{-2}St^{-1}Ct^{-1}$, is more appropriate than the value of about 0.008 $WM^{-2}St^{-1}Ct^{-1}$, published by MIEC. The MIEC calibration coefficient was obtained as described by Schmetz (1989). The method is based on applying the radiative transfer equation to temperature and humidity data from radiosondes and then comparing the computed radiances (in physical units) with the observed radiances (in counts). It is noted with considerable interest that a calibration coefficient some 17% below the MIEC value was obtained by Gärtner (1990) by comparing the counts obtained for very high, thick clouds in the IR and WV channels. This approach is much closer in philosophy to that of the vicarious method and it is very revealing that such similar results are obtained. Therefore a thorough consideration of possible reasons for the discrepancy is given below. It is considered easier to explain the relatively small difference between Gärtner's calibration and our own (which is probably within the combined experimental error of the two methods) than it is to explain the relatively large difference between Gärtner's calibration and the MIEC value.

5.3 Possible causes of the discrepancy between the MIEC water vapour channel calibration coefficient and the vicarious value

5.3.1 Inconsistent emissivities at infra-red and water-vapour channel wavelengths

Szejwach(1982) reports aircraft measurements which imply that the emmisivities at the two wavelengths agree to within 6%. However this figure arises from data from a single aircraft flight, which may have been over an unrepresentative cloud, and the data shown in the paper suggest that at high emissivities the IR emissivity is greater than that at WV channel wavelengths. Higher emissivities at IR wavelengths than at WV wavelengths are needed to explain the discrepancy. Schmetz (1992) concedes that small particles may have just that effect on the ratio of the emissivities.

5.3.2 Anomalous radiometer performance at the time of the I.C.E. experiment

The missions considered all took place during the period when eclipse was affecting the satellite, and in addition, as documented by Mason and Diekmann (1990), at the time the satellite was experiencing its first cooler and detector contamination. At the time of eclipse, the calibration of both detectors undergoes diurnal variation, and given that the MIEC calibrations of the two channels are performed at different times of day, this may be a factor. Also , as noted by Mason and Diekmann, the process of contamination undoubtedly changes the spectral response of the detectors, and this would in turn give rise to inconsistencies between the two calibrations.

5.3.3 Possible bias in radiosonde data

The radiosonde humidity sensor is not as reliable at low temperatures as it is at high temperatures, and clearly any bias in the humidity at the levels where water vapour channel radiances would be affected would, in turn, affect the MIEC calibration. If the radiosondes consistently underestimated the humidity in the upper troposphere, this could explain the discrepancy.

5.3.4 Inconsistency between radiative transfer models used at ESOC and the UK Met Office

Both the MIEC calibration and the vicarious calibration rely on radiative transfer models (as described by Schmetz (1989) and LOWTRAN-7 (Kneizys et al,1988) respectively), and clearly if these were inconsistent the discrepancy could be explained. Therefore a test was performed in which the opaque cloud curve used in the semi-transparency correction was calculated using both models. It was found that the differences were very small and not in the right sense to explain the discrepancy in WV channel calibration.

5.3.5 The presence of aerosols

The radiative transfer models have to be given information about the aerosol content of the atmosphere. Clearly if this information is incorrect, particularly in respect of aerosols which absorb differently at 6μ and 11μ, an inconsistency would result.

5.3.6 Large amounts of anthropogenic water vapour in the low stratosphere

Foot (1984) has documented measurements of humidity in the low stratosphere in the U.K. area (and northwards) using aircraft measurements made in the 1970s. If the mean values he found still pertain today then it seems unlikely that this is a significant factor in the discrepancy. However, in addition to the general uncertainty in the amount of water vapour in the low stratosphere, there is uncertainty as to whether it is remaining constant in time, or possibly increasing. Anthropogenic sources, specifically sub-sonic aircraft, could be causing a significant increase. Grassl (1990) comments:

> If from the yearly consumption of 120 million tons of aviation fuel resulting in 150 million tons of water vapour 20 percent are injected into the stratosphere northward of 40^0 N (Lufthansa gave 15-17 percent for a test under summer conditions) this constitutes 15 percent of the typical water vapour content of the 10 to 13 km layer for the area north of 40^0 N. For this calculation a mixing ratio of 4 ppm has been assumed. Taking a residence time (here e-folding time) of one year a 5-6 percent increase in the 10 to 13 km layer would result.

Paradoxically, this effect may well be at a maximum over the North Sea and therefore may well have significantly affected results using I.C.E. data. Due to the utilisation of the North Atlantic Organised track Structure (e.g. Nolan, 1990) a relatively large percentage of the sub-sonic flights in the low stratosphere will be in U.K. airspace and the resulting water vapour will be advected by the prevailing winds over the North Sea.

5.3.7 Uncertainty in the spectral response of the WV channel

Both the MIEC method and the vicarious method rely on knowlege of the spectral response of the WV channel but in different ways. Therefore if the published spectral response (ESOC, 1989) is incorrect this could in principle explain the discrepancy. There is apparently some uncertainty in the response which could contribute to the inconsistency (but could probably not explain it all by itself).

5.4 Inherent uncertainties in the semi-transparency correction

If the only source of error in the semi-transparency correction was the calibration of the WV channel, one approach which might seem attractive would be to use a slicing approach, as in, for example, Smith and Frey (1992). This technique also constructs a line in a two-dimensional histogram, but unlike the technique used at ESOC, only the slope of the line is used, not its absolute position (which depends critically on the calibration). However it is important not to underestimate the uncertainty in the slope of this line. This is illustrated in figure 5.1. This was constructed by considering every point in the background cluster (for which there was at least one pixel having that combination of values) and constructing a straight line to every point in the cloud cluster. The line is then extrapolated to a fixed value in IR counts. In constructing this diagram, no empirical re-registration, as described above, was applied. As can be seen, the spread of possible lines is extremely large, and it is asserted that the uncertainty in the specification of the straight line is in fact the dominant source of error in the semitransparency correction. It is noted though that the operational semi-transparency correction

has a number of checks on such variables as the slope of the line, which mean that if the line adopts one of the extreme values illustrated, no correction is applied.

Nevertheless, because of the uncertainty in the specification of the line, it is argued that the use of an artificially high value of the WV channel calibration coefficient can produce better height assignment than the use of a value which might be obtained from a vicarious procedure, such as outlined above. The reasoning is as follows. If an artificially high value of the calibration coefficient is used this leads to the semitransparency correction not being applied on a large number of occasions, because, given the IR radiance (in counts), the WV channel radiance (in counts) is greater than the corresponding number on the opaque cloud line. In these circumstances, the uncertainty in the slope of the straight line does not have any deleterious effects. As described by Schmetz et al (1992) and confirmed by Woick (1992) the quality of ESOC's winds improved in September 1987 after the introduction of the new WV channel calibration scheme, as a result of which higher calibration coefficients were used. It is considered that this can be explained by the above argument.

It can be argued that, rather than produce a diagram like figure 5.1, it would be better to quantify *all* the sources of error in the semi-transparency correction. The difficulty with this is that it is impossible to calculate the errors in a consistent way. For example, there is uncertainty in the opaque cloud line stemming from a number of areas, many of which are mentioned in the previous subsection. However quantifying these sources is almost impossible, certainly in a way which would be consistent with the way in which the uncertainty in the straight line is quantified.

5.5 Results of tests with different WV channel calibration coefficients

Because it was hypothesised that the semitransparency correction can, potentially, function more effectively if the value of the WV channel calibration coefficient is higher than vicarious calibration would suggest, it was decided to perform the height assignment of the SCMWs generated for the I.C.E. experiment using a range of possible coefficients. The range chosen was from 0.0050 $WM^{-2}St^{-1}Ct^{-1}$ to 0.0085 $WM^{-2}St^{-1}Ct^{-1}$, in steps of 0.0005 $WM^{-2}St^{-1}Ct^{-1}$. Winds were verified for all five template sizes under consideration, and in addition, for the four smaller template sizes, the semi-transparency correction was applied both using radiances on the scale in question and using the radiances for the 32 * 32 segment. Verification was performed by comparing the wind using the prescribed height assignment with the wind derived from the aircraft wind at that level, and the root mean square vector difference was calculated. The results are given in the following table (RMS vector differences in pixels per half hour). The results are for all the missions and times specified in the earlier table.

Table 5.2 : *RMS vector differences for various scales and calibrations*

Scale of Wind	*Scale of Semi − transparency Correction*	*WV channel calibration coefficient* $WM^{-2}St^{-1}Ct^{-1}$							
		.0050	.0055	.0060	.0065	.0070	.0075	.0080	.0085
8 * 8	32 * 32	3.67	3.67	3.67	3.67	3.66	3.66	3.66	3.66
8 * 16	32 * 32	3.55	3.56	3.55	3.55	3.54	3.54	3.54	3.54
16 * 16	32 * 32	3.45	3.45	3.42	3.39	3.37	3.36	3.36	3.36
16 * 32	32 * 32	3.17	3.21	3.15	3.11	3.07	3.06	3.06	3.06
32 * 32	32 * 32	2.22	2.15	2.06	2.06	1.87	1.84	1.86	1.92
8 * 8	8 * 8	2.43	2.30	2.21	2.21	2.19	2.17	2.18	2.18
8 * 16	8 * 16	2.16	2.10	2.02	1.96	1.93	1.93	1.96	1.97
16 * 16	16 * 16	2.45	2.20	2.11	2.12	2.08	2.04	2.04	2.03
16 * 32	16 * 32	2.20	1.97	1.88	1.92	1.87	1.83	1.79	1.77

From the above table it can be concluded that the use of a high WV channel calibration coefficient produces better results than a low coefficient, with little to chose between .0080 and .0085. As far as scale is concerned, the best results in terms of RMS vector error were produced using a 16 * 32 array both to track the cloud system, and to perform the semi-transparency correction. However, the fact that using a 16 * 16 array produces worse results than either of the two neighbouring scales is difficult to explain, and is thought to stem from the relatively small sample used. It should be born in mind that even though a relatively small scale may produce worse statistics than a larger one, there may be useful information implicit in the enhanced resolution. Therefore the conclusion from this part of the study is that *probably* the best scale to use is 16 * 16. Of course if it proves feasible to produce winds with a 16 * 16 array of visible channel data, this will have the effective resolution of an 8 * 8 array of IR data. It should be borne in mind that, even if the semi-transparency correction and tracking are performed with a 16 * 16 array, significant processing will still be carried out on a 32 * 32 array, specifically the histogram interpretation and the selection of the peak in the correlation surface used to guide selection at smaller scales.

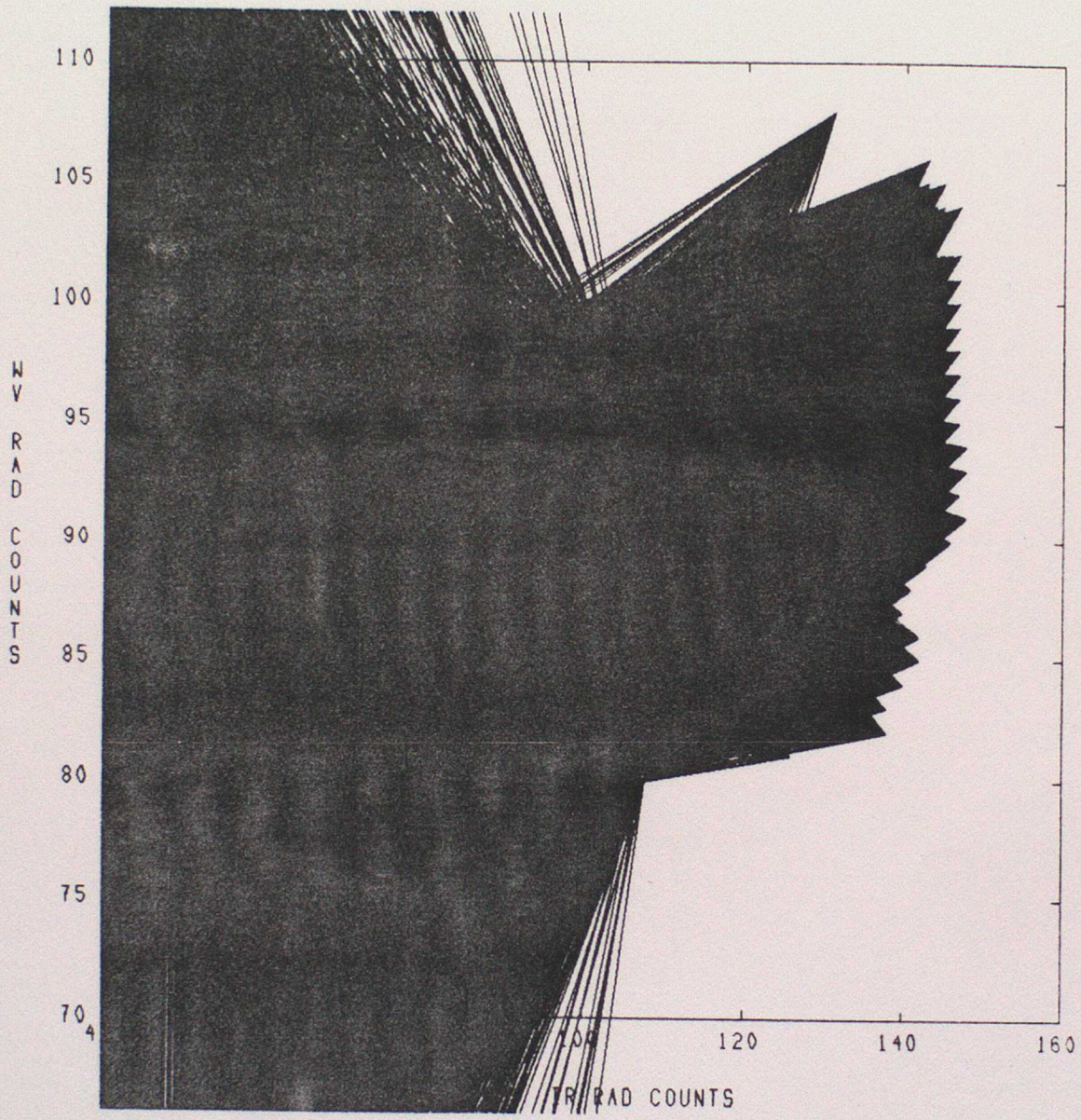

FIGURE 5.1 ILLUSTRATES UNCERTAINITY IN "STRAIGHT LINE" OF SEMI-TRANSPARENCY CORRECTION (SEE TEXT FOR EXPLANATION)

6 Recommendations for the calibration/validation of winds and radiances

6.1 Relative merits of using aircraft data and radiosonde data as ground truth

Subsequent parts of this section discuss proposals for using radiosonde data and, quite separately, aircraft data in calibration/validation exercises. It is worth stressing the relative merits of each data source, as both have their relative merits and limitations. Radiosonde data are available routinely and there is a good chance that, during the life of a satellite, radiosondes will sample almost every type of profile that is likely to occur. On the other hand, in general radiosondes certainly do not measure radiances which could be used to calibrate the radiometers directly, and it can be argued as to whether what radiosondes measure can be directly compared with quantitative products derived from METEOSAT data. Aircraft can carry radiometers and, if appropriately instrumented, can measure almost any required parameter: the main limitation is one of sampling. Designing an experiment to make measurements of a specific phenomenon, for example, a cirrus cloud with a significant amount of vertical windshear, is quite difficult, and even if such a phenomenon was perfectly predictable, much flying would be needed to generate a representative dataset. Therefore it is considered that both aircraft and radiosonde data have a role to play in calibration/validation of METEOSAT quantitative products, and they are addressed in turn.

6.2 The use of radiosonde data

It would be perfectly possible to produce ELBFs using radiosonde data. However, a major limitation of the sonde data is that they are only representative of scales of a few kilometers, and as the cross-sections show, if a small scale wind is used in the height attribution, a serious error can result. Note that if the isopleths of wind component slope at 1 in 60, as was shown in section 3.4, having a single radiosonde displaced from the centre of the segment by 150km would give rise to a height assignment error of 2.5km. The use of numerical analyses is a possibility, but these data sets have quirks of their own and cannot be regarded as being independent of the satellite data. What is recommended is that very careful use is made of radiosonde data, in particular, quantitative products are compared with the average of at least two radiosonde profiles. In order to facilitate this, the concept of tailored segments must be invoked, that is, segments must be designated such that at least two radiosonde stations lie inside them. Figure 6.1 illustrates the feasibilty of this. It shows all sonde station pairs within Europe such that, in the METEOSAT space view projection, the x coordinates of the stations differ by less than 32 pixels, and so do the y coordinates. Also shown are the 32 * 32 segments which are centred on the midpoint between the stations. Although there will be occasions when, for example, a jet core passes between two stations and thus the average wind from the two stations is not representative, this will be rare and the consequences of it can be quantified.

Note that such an approach would almost certainly have benefits for the calibration of the water vapour channel. The representativeness of a radiosonde humidity profile is significantly less than that of a wind profile. However, it is not believed that the use of a single humidity profile contributes to the bias in the water vapour channel calibration.

As was stated earlier, these conclusions should be regarded as tentative and the recommendations as provisional. The results confirm that there is significant vertical and horizontal shear in cirrus cloud and that the empirical level of best fit does not agree with the level resulting from applying the semi-transparency correction. This is consistent with the view that the height assignment is a major source of error: clearly if there was little vertical shear in the cloud, then an erroneous height assignment would not give rise to an erroneous wind vector. The semi-transparency correction is very susceptible to the quantity of radiance data supplied to it: only if cloudy and cloud-free air are both well-sampled can the correction be accurately calculated.

6.3 Dedicated experiment with C-130 to improve our understanding of semi-transparency correction

In the EUMETSAT-sponsored study of I.C.E. aircraft data, only the wind, temperature and humidity information from the French and German aircraft were used. Given that one can obtain those parameters from C-130 dropsondes, a possibility for a future experiment is to use the C-130 by itself, making both in situ and dropsonde measurements. Such an experiment could then be a one-off, or a few-off, rather than part of a major international experiment. This would facilitate an experimental design which more closely reflected the operational production of SCMWs.

Specifically what is proposed is that an individual experiment would focus exclusively on an individual MIEC segment. The MIEC segments in which the dropping of dropsondes has been successfully demonstrated are shown in figure 6.2: clearly any of them could be reached within a day's flying of Farnborough (or Boscombe). The experiment would consist of dropping dropsondes close to the four corners of one segment and making, within the segment, in-situ measurements, primarily of upwelling radiation at wavelengths corresponding to the METEOSAT infra-red and water-vapour channels. These measurements would be made at dropsonde release altitude, i.e. as high as possible. It is considered that, for temperature and wind, and to a lesser extent humidity, measurements at the corners can be interpolated to give conditions inside the segment, but for radiative and microphysical properties significantly more observations are required. The complexity of the experiment is constrained by two opposing considerations. The images used to generate an SCMW span a period of an hour (typically from 1020GMT to 1120GMT for the 'midday' winds) so measurements made outside that hour period will be more difficult to compare with the satellite data. Furthermore, in order for the C130 to get as high as possible the minimum amount of fuel should be loaded, so a short mission is to be preferred.However, to make representative in situ measurements over an area of 150km by 300km using an aircraft moving at 300 knots would take well over an hour if done properly.

The suggested compromise is to fly a pattern comprising the two short sides of the segment and the diagonals. A consideration in this design is as follows. Following the release of a dropsonde, the C130 must fly essentially straight until the sonde hits the water, and this takes about 20 minutes, corresponding to 180km of flying in still air. (Straight flight is necessary because if the aircraft banks significantly the signal from the dropsonde can be lost). This makes flying the short sides of the segment non-trivial. However, given that the experiment will only be worth performing if there is significant vertical wind shear, and that such shear normally occurs in a westerly situation, it is reasonable to assume that there would be a significant headwind component when flying westwards along the short sides of the segment. Provided the equivalent headwind is 50knots or greater, the sonde will have hit the water before the aircraft reaches the western edge of the segment. Of course, in order to have a headwind when flying both short sides of the segment, it is necessary to fly a diagonal in between. Flying diagonals also has the advantage that in situ measurements are made well inside the segment, which is clearly desirable. A fifth dropsonde near the centre of the segment would be desirable. Figure 6.2 shows such a pattern for an eminently plausible segment.

Assuming that the experiment is timed to be contemporaneous with the midday SCMW extraction, and that the sondes are dropped at the corners of the segments, then, for a particular segment, the times and locations of the sonde releases are determined well in advance. It is hoped that this predictability will make the experiment more appealing to the air traffic control authorities. However, it is still desirable to have considerable flexibility on the day. For example, just before dropping the second sonde it would still be possible to focus the experiment on the segment immediately to the north of that indicated on figure 6.2, if the latest information suggested it was a better prospect. Some east-west flexibility could usefully be exploited as well: the possible waste of a sonde would be worthwhile. The decision as to which segment has the most suitable cloud conditions is best made on the ground, by someone with access to satellite imagery, possibly even at ESOC. Some tests would have to be performed as to how accurately we can predict whether a segment will have cloud appropriate to SCMW extraction, on the timescales required by the air traffic control authorities. Clearly there will have to be occasions when the airspace is booked but the mission is aborted because the cloud conditions are inappropriate.

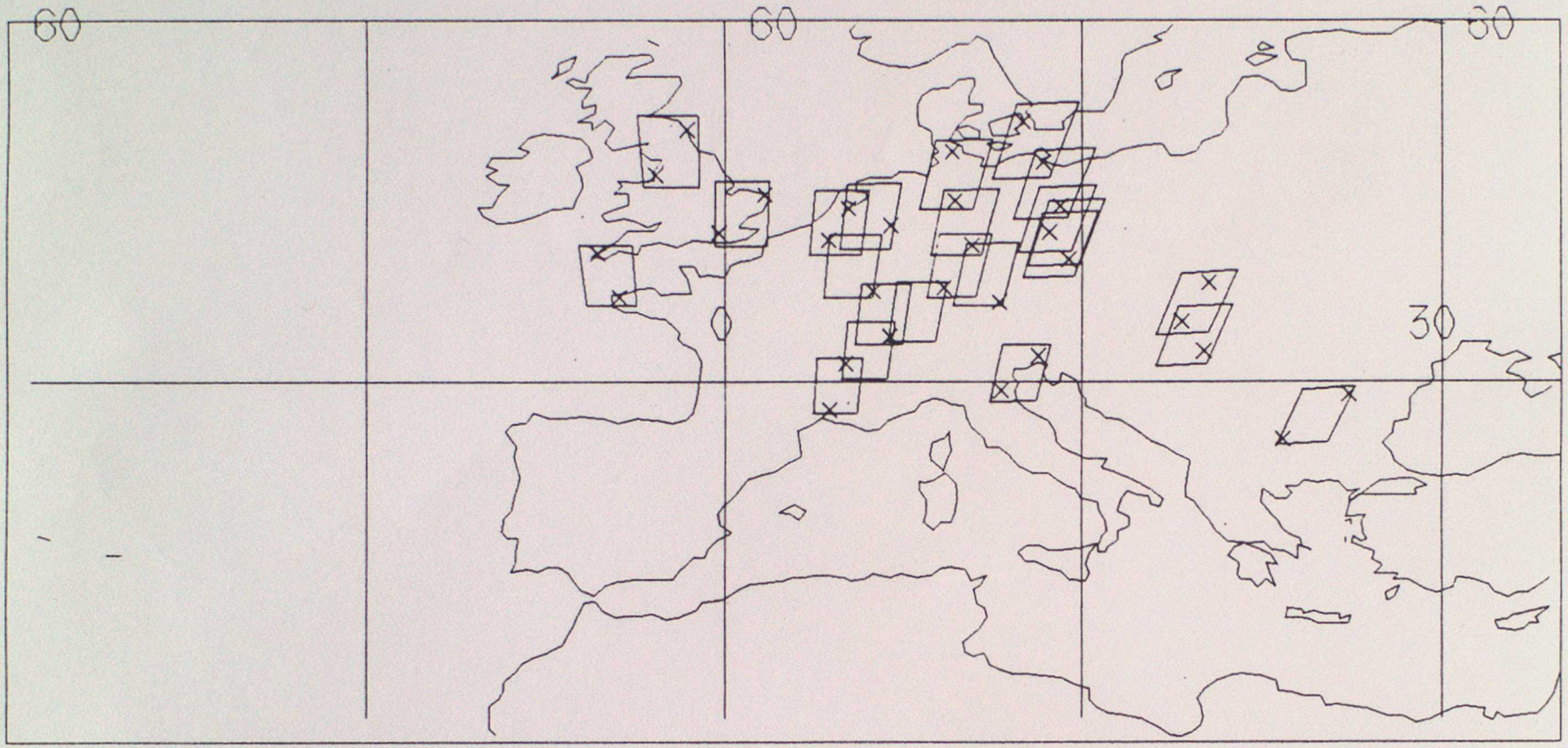

FIGURE 6.1 SHOWS POSSIBLE 32*32 PIXEL SEGMENTS WITHIN EUROPE CONTAINING AT LEAST 2 RADIOSONDE STATIONS,TOGETHER WITH THOSE STATIONS

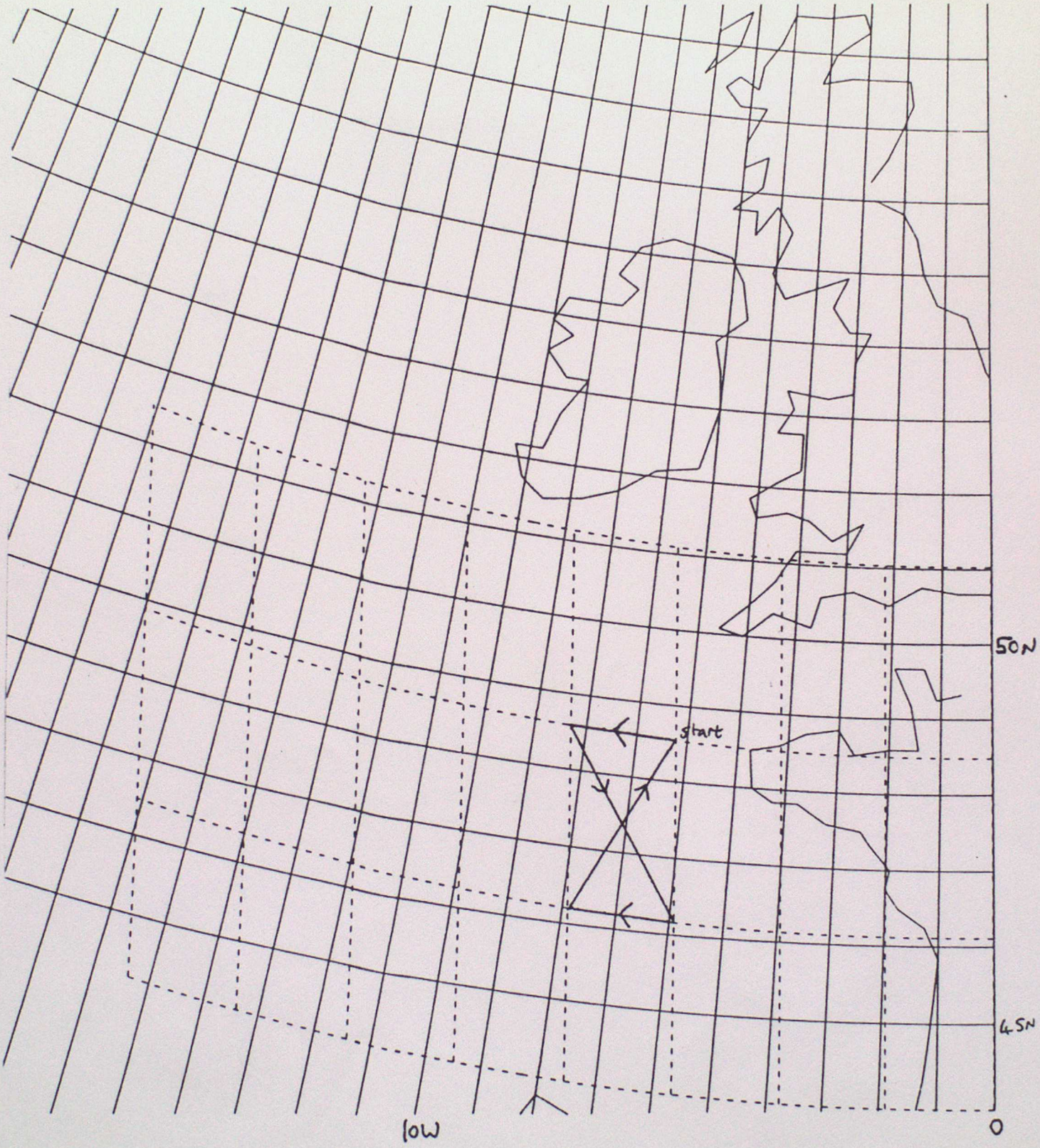

FIGURE 6.2 SHOWS MIEC SEGMENTS ACCESSIBLE BY C-130 AND PROPOSED EXPERIMENTAL FLIGHT PATTERN IN ONE

7 Comments on future approaches to the height attribution of semi-transparent clouds

An alternative approach to the semi-transparency correction is as follows. Historically, producing SCMWs from semi-transparent clouds has been regarded as a variation on the theme of SCMW production from opaque clouds. In addition winds have been produced by tracking humidity features in water-vapour imagery, wherein it is recognised that the resulting vector is a weighted mean of the wind vector over some depth of the atmosphere. It is perhaps then better to regard the production of SCMWs from semi-transparent clouds as a variation on the theme of wind extraction from absorption channel imagery. It has been shown using simulated water vapour channel radiances that it is possible to produce a number of winds, with different weighting functions, by filtering the radiances before applying cross-correlation techniques (Lunnon, 1992). The weighting functions are still quite broad, however, but the presence of a layer of semi-transparent cloud would sharpen the weighting functions considerably. What is recommended then is that a number of simulations are performed to determine the characteristics of the weighting functions in the presence of cloud. The way the semi-transparency correction would be applied in practice would be as follows. Following the extraction of a wind using infra-red imagery, a number of winds would be extracted using water vapour imagery, with different filterings of the basic radiances. The water-vapour channel wind which best agreed with the infra-red channel wind would then be considered. The simulations would tell us what was the appropriate temperature range of the weighting function, and this information would be the basis of the height assignment. The information from the IR/WV histogram, which is the basis of the present semi-transparency correction, would be used to select which of the simulations would be appropriate. The data from the I.C.E. experiment would form an excellent test-bed for any proposed new correction.

Acknowledgement

- To EUMETSAT, for sponsorship, and allowing the contract timetable to be extended.
- To ESOC, for provision of satellite imagery and software
- To DLR, for provision of Falcon data
- To LMP, for provision of Merlin data
- To MRF, for provision of C-130 data

Appendix

On the generation and selection of model atmospheres for use in radiative transfer calculations.

In order to implement the semi-transparency correction it is necessary to have a representation of the functional dependence of water-vapour (WV) channel radiance against infra-red (IR) channel radiance for opaque clouds at a variety of heights in the atmosphere. Such a dependency is a function of the profile of temperature, humidity, trace gas concentration and aerosol distribution. In practice the effects of aerosols and trace gases are treated rather crudely and the important consideration is the treatment of the combined effects of humidity and temperature. If the atmosphere was completely dry and uniformly mixed gases did not contribute to the absorption in the parts of the spectrum viewed by the IR and WV channels, then the dependency would simply reflect the Planck functions at the different wavelengths. The maximum departure from the dry atmosphere case occurs when the atmosphere is saturated, and it can be shown that, for saturated atmospheres, the sensitivity to details of the temperature profile is rather small. Thus effort should be concentrated on determining the dependence on relative humidity. It is also important that, given a set of model atmospheric profiles and a real profile, a simple and reliable method exists for selecting the model profile whose radiative properties most closely resemble those of the real profile. One potential problem is the variability of the height of the slab of the atmosphere whose humidity is important in determining the radiative properties: for example in the mid-latitude winter profile used operationally, the contribution function peaks at $6km$, whereas for the tropical profile the peak is at about $9km$. It was therefore decided to use downward integrated water vapour amount as one of the coordinates which would be used in the indexing system. This is defined to be either $\int \rho_v dz$ or $\frac{1}{g}\int m dp$, where ρ_v is the vapour density and m is the humidity mixing ratio. In practice the integral is always multiplied by the secant of the satellite zenith angle. A more difficult issue is the question of what the limit of the integral is, i.e. what is the altitude above which absorption can be ignored. It should be stessed that the WV channel transmittance changes very quickly through the uppermost layers of water vapour in the atmosphere: the transmittance to space at a zenith angle appropriate to the north sea can be reduced to 0.76 by the passage through $0.12kgm^{-2}$ of *vertically* integrated water vapour. Thus the choice of whether that uppermost layer is in the stratosphere or the troposphere is a significant one. What is imperative is that consistency is maintained between any assumptions used, for example, to calibrate the water vapour channel, and those assumptions used in the generation of model profiles. For the operational semi-transparency correction, this appears to be the case: in all pertinant calculations it is assumed that forecast or observed relative humidities can be used without modification below $300mb$, between $300mb$ and $100mb$, relative humidities are interpolated between the $300mb$ value and zero at $100mb$, and above $100mb$ the atmosphere is assumed dry. However, in the present work the method of indexing the model profiles was to assume that each consisted of a number of slabs of constant relative humidity air, overlaid by a dry stratosphere. The tropopause was assumed to be at $200mb$, as the temperature profile used suggested that altitude. As was suggested earlier, the boundaries of the slabs would be at points having particular values of downward integrated water vapour amount. Thus if the top slab had a relative humidity of 25%, it would extend further down in to the atmosphere than it would if it had a relative humidity of 50%. The relative humidities of the slabs were either $12\frac{1}{2}\%, 25\%, 50\%$ or 100%. Three slabs were considered, so the number of model profiles was 64. Although a profile in which there is a slab of air with a relative humidity of $12\frac{1}{2}\%$ adjacent to a saturated layer may seem unusual, in the presence of cloud strong vertical gradients of humidity can occur, so they should be catered for. The boundaries of the slabs were at downward *vertically* integrated water vapour amounts of 4.87, 12.96 and $42.96kgm^{-2}$(however note that the radiative transfer calculations are performed using a satellite zenith angle appropriate to the north sea). For a saturated atmosphere, the levels at which these boundaries occur are at $244mb, 312mb$ and $397mb$ respectively. The temperature profile used in this, and indeed all calculations, is one typical of the middle of the experimental area for mission 207, i.e. 28th September 1989. Thus selecting the model atmosphere is a simple process. The vertically integrated water vapour is calculated, and the mean relative humidities of the 3 slabs calculated, the logarithms of those relative humidities derived, and those logarithms used as indices to address the appropriate profile. Model 1 is one where the relative humidity is around $12\frac{1}{2}\%$ everywhere, while model 64 is saturated everywhere. The model number is equal to

$$index1 + 4 * index2 + 16 * index3 + 1,$$

where index1 relates to the humidity in the uppermost layer, index2 relates to the intermediate layer and index3 relates to the lowest layer.

Two figures illustrate the opaque cloud curve for various model atmospheres. Figure A.1 shows the curves for the five profiles having constant relative humidity. Figure A.2 shows the curves for the models selected

for the 8 * 8 templates comprising a single segment at a particular time. This was produced to illustrate the variability of the opaque cloud curve within a MIEC segment.

References.

Bell, R.S. and Dickinson, A. 1987 The Meteorological Office operational numerical weather prediction system *Met Office Scientific Paper No 41 HMSO*

Bowen, R.A. and Saunders, R.W. 1984 The semitransparency correction as applied operationally to METEOSAT infra-red data: A remote sensing problem. *ESA Journal* 8 (2), 125

Coakley, J.A. and Bretherton, F.P. 1982 Cloud Cover from High Resolution Scanner Data: Detecting and allowing for partially filled fields of view *J. Geophys Res.* 87 4917–4932

Diekmann, F.J. and Amans, V. 1990 On the radiometric and geometric quality of METEOSAT images in *Proceedings of the 8th METEOSAT Scientific user's Meeting, Norrkoping, August 1990. published by EUMETSAT, EUM P 05*

ESOC 1989 METEOSAT-4 calibration report, Issue 3 and Annexe. Available from ESOC, Robert Bosch Strasse 5, Darmstadt

ESOC 1990 METEOSAT-4 calibration report, Issue 4. Available from ESOC. Robert Bosch Strasse 5, Darmstadt

Foot, J.S. 1984 Aircraft measurements of the humidity in the lower stratosphere from 1977 to 1980 between 45° N and 65 ° *Q J R Meteorol Soc.* 110 303–319

Gärtner, V. 1990 Intercalibration tests for the METEOSAT WV and IR channels in *Proceedings of the 8th METEOSAT Scientific user's Meeting, Norrkoping, August 1990. published by EUMETSAT, EUM P 05*

Grassl, H. 1990 Possible climatic effects of contrails and additional water vapour in *Air Traffic and the environment - Background, Tendencies and Potential Global Atmospheric Effects, Proceedings of a DLR International Colloquium Bonn, Germany, November 1990, published by Springer-Verlag*

Holmlund, K. 1992 Tracer quality indicators for accurate cloud motion wind estimates in *Proceedings of a workshop on wind extraction from operational meteorological satellite data, Washington, U.S.A.. September 1991, published by EUMETSAT*

Hoskins, B.J. and Pedder, M.A. 1980 The dignosis of middle latitude synoptic development *Q J R Meteorol Soc,* 106 707–720

Kneizys, F.X. et al 1988 Users guide to LOWTRAN 7 *AFGL-TR-88-0177 Environmental Research Papers No 1010, Air Force Geophysics Lab, Hanscom AFB, MA 01731*

Laurent, H. 1992 Wind extraction from multiple METEOSAT channels in *Proceedings of a workshop on wind extraction from operational meteorological satellite data, Washington, U.S.A., September 1991, published by EUMETSAT*

Lunnon, R.W. and Lowe, D.A. 1990 How accurately can we predict the errors in satellite cloud motion winds? in *Proceedings of the fifth AMS conference on satellite meteorology and oceanography, London, September 1990*

Lunnon, R.W. 1991 Short range forecasts for air traffic control using high resolution aircraft data. in *Proceedings of fourth international AMS conference on the aviation weather system, Paris, June 1991*

Lunnon, R.W. and Lowe, D.A. 1991 A study of different methods of interpolating numerical forecast data for the purpose of validating cloud motion winds. in *Proceedings of a workshop on wind extraction from operational meteorological satellite data, Washington, U.S.A., September 1991, published by EUMETSAT*

Lunnon, R.W. 1992 Profiles of wind using time-sequences of absorption channel imagery from geostationary satellites: proof of concept using synthetic radiances. *Short Range Forecasting Research Division Technical Report No 29, available from Meteorological Office*

Lunnon, R.W. and Lowe, D.A. 1992 Spatial scale dependency of errors in satellite cloud track winds. *Advances in Space Research* 12 No 7 127

Mason, B.D. and Diekmann, F.J. 1990 IR detector contamination - causes and effects **in** *Proceedings of the 8th METEOSAT Scientific user's Meeting, Norrkoping, August 1990. published by EUMETSAT, EUM P 05*

Nolan, M.S. 1990 Fundamentals of air traffic control *Wadsworth publishing company*

Schmetz, J. 1989 Operational calibration of the METEOSAT water vapour channel by calculated radiances *Applied Optics* **28** 3030–3038

Schmetz, J. 1992 Further improvements of cloud motion wind extraction techniques **in** *Proceedings of a workshop on wind extraction from operational meteorological satellite data, Washington, U.S.A.. September 1991, published by EUMETSAT*

Schmetz, J., Holmlund, K., Hoffman, J., Strauss, B., Mason, B., Gärtner, V., Koch, A. and Van de Berg, L. 1992 Operational cloud motion winds from METEOSAT infrared images. *submitted to J Appl Meteorol*

Smith, W.L. and Frey, R. 1992 Altitude specification of cloud motion winds **in** *Proceedings of a workshop on wind extraction from operational meteorological satellite data, Washington, U.S.A., September 1991, published by EUMETSAT*

Szantai, A. and Desbois, M. 1992 Wind extraction and validation from the water vapour channel of METEOSAT during the International Cirrus Experiment **in** *Proceedings of a workshop on wind extraction from operational meteorological satellite data, Washington, U.S.A., September 1991, published by EUMETSAT*

Szejwach, G. 1982 Determination of semi-transparent cirrus cloud temperature from infra-red radiances: Application to METEOSAT *J Appl Meteor* **21** 384–393

Thorpe, A.J. and Clough, S.A. 1991 Mesoscale dynamics of cold fronts: structures described by dropsoundings in FRONTS87 *Q J R Meteorol Soc,* **117** 903–942

Thoss, A. 1992 Cloud motion winds, validation and impact on numerical weather forecasts **in** *Proceedings of a workshop on wind extraction from operational meteorological satellite data, Washington, U.S.A.. September 1991, published by EUMETSAT*

Wilson, G.S. 1984 Automated mesoscale wind fields derived from GOES satellite imagery. *Amer. Met. Soc. Conf. Sat./Remote Sens. Appl.* 164

Woick, H. 1992 Verification of cloud motion winds **in** *Proceedings of a workshop on wind extraction from operational meteorological satellite data. Washington, U.S.A., September 1991, published by EUMETSAT*